We thank referee #1 for their thoughtful comments and reply to each in turn below:

Potential changes in community structure during 50-55 h incubations:
In the attached Figure (which we plan to add to the Supplementary Material) we show data from Incubation 1, where subsampling took place at 29 h and 52 h (these data were not previously shown). It is evident that the changes observed at 52 h were already underway at 29 h, and in some cases had already taken place, e.g. the majority of data points for $NPQ_{SV}(1000)$. We only subsampled this one experiment at 29 h and chose the 50-55 h incubation times for all other experiments due to the low sea water temperature (as low as ~10C), which would increase physiological response times compared to temperate waters. If we assume a growth rate no higher than 0.28 d-1 for the subantarctic zone (e.g., see Ryan-Keogh et al. 2018, Table 2), then the phytoplankton community would not have doubled over 50 hours. We thus conclude that 50-55 h is not enough for a significant change in the community composition, and also point to the attached figure as evidence that the overall trends found after 52 hours were generally consistent with those found at 29 h but are more pronounced. Conducting the longer incubations is thus unlikely to have biased the conclusions.

CHEMTAX vs Diagnostic Pigment Index:
We chose the Diagnostic Pigment Index over CHEMTAX because it assumes less *a priori* knowledge specific to an oceanic region. CHEMTAX is only as good as the comparison matrix that is specified for it, and as far as we are aware, there is no available matrix specific for the Subantarctic Zone. CHEMTAX would produce a result regardless, but possibly not a very accurate one – without microscopy to match, it would be difficult to know whether the result is valid. In order to avoid overstating what our data can do, we thus decided to show the pigment composition (Figures S2 and S3), which is the raw, unbiased data, and to provide a metric for the community composition with the Diagnostic Pigment Index, while also discussing its suitability in the region and comparing our results to those found previously at the SOTS site.

Average mixed layer irradiance in the two water masses and its influence on NPQ:
We disagree with the notion that the average light field is the main determinant of NPQ. When realistic vertical mixing is simulated, it appears that low-light (deep ML)-acclimated cells display a larger capacity for NPQ than high-light (shallow ML)-acclimated cells (e.g. Milligan et al. 2012). This phenomenon was likely overlooked in earlier laboratory studies because realistic mixing regimes were rarely simulated.
Regardless, we are happy to include estimates of daily integrated median underwater PAR for the respective mixed layers for reference. They are calculated for the nominal date of March 30, 2018, with Kd_PAR estimated as a function of Chl following Morel et al. (2007). The results are as follows: For the warm regime (average Chl=0.62 mg m-3 and MLD = 100 m), the median daily mixed layer PAR is 0.13 mol m-2 d-1. For average Chl = 0.38 mg m-3 and MLD=20 m and MLD=90 m as the two extremes, the median daily mixed layer PAR is 15 and 0.5 mol m-2 d-1, respectively. We propose to include these numbers in section 3.2.2 with an expanded subtitle: Mixed layer depths and average light field.

Paragraph starting line 455, Rates of water column integrated primary productivity (PP) and their dependence on phytoplankton biomass, temperature, and light availability:

A comparison between the conditions reported by Westwood et al. (2007) and found in our study shows the following: Sea surface temperatures were similar (12C vs 11C, respectively), mixed layer depths were also similar (mean=38 +/- 11 m and mean=35 +/- 1 m, respectively), but the column-integrated Chl was different: mean=46 +/- 11 mg m-2 vs mean=13 mg m-2. However, the fact that biomass was lower in our study could also be the result of lower iron concentrations (and less primary productivity). Moreover, normalizing the mean column-integrated PP for each study by the mean column-integrated Chl concentration yields 85 mg C (mg Chl)-1 d-1 for Westwood et al. and 31 mg C (mg Chl)-1 d-1 for our study, indicating that the Chl-normalized PP was lower during our study (in Austral fall) than in the Westwood et al. study in Austral summer. The conclusion that PP was lower in our study thus holds, with iron limitation a probable cause, as discussed in Section 3.2.4. We plan to add the information provided above to the SI of the manuscript.

Line 70, reference for 90% depression of fluorescence by NPQ: Falkowski et al. 2017. We will include this reference in the text at line 70.

Section 2.2, only one replicate 250 mL sample per treatment for the incubations: There was indeed only one 250 mL sample per treatment in each incubation because measurement of all 4 treatments took ~2 h, so measurement of triplicates would have taken ~6 h. Given the sensitivity of fluorescence parameters to the time of day (i.e. to the light history experienced by the phytoplankton), we thought it prudent to stay in a 2-h time window in order to be able to compare findings between treatments. We would like to point out that we grouped the three experiments, thus having produced true triplicates. We will clarify this in Section 2.2 in the updated manuscript.

Line 174, 'optimization' of FLCs for estimates of NPQ capacity:
This comment is discussed in detail in the response to Referee #2.

Section 2.4.3, fluorometric Chl method: We followed the JGOFS 1994 recommendations for the 'Measurement of Chlorophyll a and Phaeopigments by Fluorometric Analysis', employing the acid ratio method described by Holm-Hansen et al. (1965). We will add this detail to the section indicated.

Line 508, add reference to Figure 8: we will add this figure reference as suggested.

We thank referee #2 for their thoughtful comments and reply to each in turn below:

Line 336: description of a 'decrease in NPQ capacity' with Fe addition:
The language regarding "NPQ capacity" in this manuscript is in line with the way that Schuback and Tortell (2019) use the term, so we suggest to keep the terminology. But we do appreciate the comment about how the sentence could be misunderstood and thus propose to change the wording as follows:
The NPQ capacity, measured as both NPQ_SV(1000) and NPQ_NSV(1000), decreased with iron addition, most likely due to increased capacity to use absorbed light energy for photochemistry.

Changes in community structure during 55-hour incubations:
We refer to our response to referee #1. Regarding the question of whether a diatom-dominated community would have shown the same patterns: We cannot answer this question with our (haptophyte-dominated) data. However, several publications have shown similar trends to ours with respect to NPQ and Fe limitation under controlled conditions (i.e. in the laboratory or with ship-board incubations), probing a variety of species including diatoms (Schuback et al. (2015), Schuback and Tortell (2019)). The evidence thus suggests that the link between NPQ capacity and Fe status is robust across a range of phytoplankton species and thus community composition. We propose to add the information presented above to section 3.3.1.

Increase in Fv/Fm in control treatments of incubations:
An increase in Fv/Fm during incubation experiments is not an uncommon feature in Fe-limited control treatments, for example see Ryan-Keogh et al. (2018). While rarely discussed in the active fluorescence literature, it is likely the result of acclimation to more constant light conditions experienced in the incubations relative to the (constantly mixing) open ocean. Less light fluctuations and thus a less variable underwater light field would allow better allocation of (limited) resources, which could result in the observed increase in Fv/Fm.

Reference for 90% quenching of ChlF signal at midday:
Falkowski et al. 2017. We will include this reference in the text at line 70.

Section 2.1, Line 137-139: We will add that the underway line was also sampled for FRRf measurements as suggested.

Section 2.2: Justification for iron treatments in incubations:
We chose the two different Fe treatments originally to test whether an addition of 0.2 nM would have a measurable effect (compared to the 2 nM Fe treatment which should definitely be Fe-sufficient). Since the results for both Fe treatments were consistent and we were primarily interested in the contrast between iron sufficiency vs iron limitation, we decided to bundle the +Fe treatments as described in the manuscript.

Line 148: "abeam" is not a typo but a nautical term, meaning on a line at right angles to a ship's length.

Line 158-159: Incubation duration of 51.5-55 hours and possible issues arising:
See response to Referee #1 regarding community composition and the sampling that was done on Incubation 1 (including new Figure for SI).

Section 2.3, Lines 168-174: Better explanation of the light curves and what is meant by 'optimization' of FLCs for estimates of NPQ capacity (lines 173-176):
The attached Figure 1 (which we suggest to add to the SI) shows the time course of light intensities in the respective FLCs. The blue line is relevant for underway samples while the red line refers to incubation samples. The different maximum light intensities were chosen such that maximum NPQ was achieved for each set of samples, while still providing an induction curve in the FRRf that cut be fitted (at higher light intensities the fluorescence

induction curve becomes too flat to achieve a good fit). Incubation samples were able to handle higher light intensities (i.e. up to 1000 umol quanta m-2 s-1) than the underway samples (750 umol quanta m-2 s-1), most likely due to high-light acclimation in the incubator. Since we were interested in the NPQ capacity we chose our experimental design to maximize the NPQ in each sample set, rather than strive for uniformity. The NPQ trends observed in the incubations and underway samples are the same with respect to iron limitation, and we don't directly compare the absolute NPQ values between these two sample sets. The difference in the maximum light intensity should thus not introduce a bias in our interpretation.

Regarding the length of the time steps and the 'optimization' of the FLCs: Since maximum NPQ capacity was our main focus, we chose an experimental design that struck a balance between i) ensuring an induction curve fit at the maximum light intensity, ii) increasing light levels slowly enough to allow derived fluorescence yields to reach steady state (thus choosing longer time steps at high light intensities), and iii) keeping the FLCs as short as possible so that the four treatments in each incubation experiment could be measured within the smallest time frame possible (<2h) in recognition of the sensitivity of photophysiology to light history and time of day.

We propose to expand lines 169-176 with a concise summary of the information provided above, while moving some of the detail about length of light steps (lines 171-172) to the Figure caption for the attached Figure 1.

Line 168-169: 'ensure complete relaxation of all NPQ':
We will clarify this section to distinguish between fast-relaxing/dynamic NPQ and slow-relaxing NPQ that will not have relaxed after an hour of low-light acclimation. The light intensity during the low-light acclimation was around 2-5 umol quanta m-2 s-1, achieved by setting the sample in a small white LDPE bottle in the shaded corner of a small cooler, placed with an open lid in a dimly lit corner of the temperature-controlled laboratory.

Line 199, different maximum light levels for NPQ estimation:
See response above (Section 2.3, Lines 168-174….). We will include the respective light levels and the samples they refer to on lines 199/200 as suggested.

Section 3.2.4 Line 466: 'macronutrient data from one CTD in that water mass indicate that the warm SST regime was not HNLC' – how many CTDs were done in that water mass?
Only one CTD was conducted in the warm water mass and the sentence will be amended to reflect this fact as follows: '…macronutrient data from the one CTD in that water mass indicate that the warm SST regime was not HNLC'. Also see comment below re CTD locations in Figure 1.

Figure 1, CTD positions are hard to see:
This Figure has been updated (attached Figure 2) to better show the CTD positions and also distinguish between CTDs in the cold water mass (overlapping on the map, cyan squares) and the one CTD in the warm water mass (red square). The figure caption will be updated also.

Figure 2: The caption to Figure 2 will be updated to include the light levels and length of FLC curves, as suggested. However, we will not include units in the parentheses of the figure

labels as the current nomenclature is in line with that of Schuback and Tortell (2019), is clearly explained in Table 1, and would otherwise become even more unwieldy than it already is.

References:
Falkowski, P., Lin, H., and Gorbunov, M.: What limits photosynthetic energy conversion efficiency in nature? Lessons from the oceans. Philos. T. Roy. Soc. B, 372, 2-8, 2017.

Ryan-Keogh, T.J., Thomalla, S.J., Mtshali, T.N., van Horsten, N.R., and Little, H.: Seasonal development of iron limitation in the sub-Antarctic zone. Biogeosciences, 15, 4647-4660, 2018.

Schuback, N., Schallenberg, C., Duckham, C., Maldonado, M. T., and Tortell, P. D.: Interacting effects of light and iron availability on the coupling of photosynthetic electron transport and CO_2-assimilation in marine phytoplankton. Plos One, 10, e0133235, https://doi.org/10.1371/journal.pone.0133235, 2015.

Schuback, N., and Tortell, P. D.: Diurnal regulation of photosynthetic light absorption, electron transport and carbon fixation in two contrasting oceanic environments. Biogeosciences, 16, 1381–1399, https://doi.org/10.5194/bg-2018-524, 2019.

References:
Falkowski, P., Lin, H., and Gorbunov, M.: What limits photosynthetic energy conversion efficiency in nature? Lessons from the oceans. Philos. T. Roy. Soc. B, 372, 2-8, 2017.

Holm-Hansen, O., Lorenzen, C.J., Holmes, R.W., and Strickland, J.D.H.: Fluorometric determination of Chlorophyll, ICES J. Mar. Sci., 30, 3-15, 1965.

Milligan, A., Aparicio, U., and Behrenfeld, M.: Fluorescence and nonphotochemical quenching responses to simulated vertical mixing in the marine diatom Thalassiosira weissflogii. Mar. Ecol. Progr. S., 448, 67–78. https://doi.org/10.3354/meps09544, 2012.

Morel, A., Huot, Y., Gentili, B., Werdell, P.J., Hooker, S.B., and Franz, A.B.: Examining the consistency of products derived from various ocean color sensors in open ocean (Case 1) waters in the perspective of a multi-sensor approach, Remote Sens. Environ., 111, 69-88, 2007.

Ryan-Keogh, T.J., Thomalla, S.J., Mtshali, T.N., van Horsten, N.R., and Little, H.: Seasonal development of iron limitation in the sub-Antarctic zone. Biogeosciences, 15, 4647-4660, 2018.

Westwood, K. J., Griffiths, F. B., Webb, J. P., and Wright, S. W.: Primary production in the Sub-Antarctic and Polar Frontal Zones south of Tasmania, Australia; SAZ-Sense survey. Deep-Sea Res. Pt. II, 58, 2162–2178, 2007.

Diel quenching of Southern Ocean phytoplankton fluorescence is related to iron limitation

Christina Schallenberg[1], Robert F. Strzepek[1], Nina Schuback[2], Lesley A. Clementson[3], Philip W. Boyd[1,4], Thomas W. Trull[1,3]

[1]Antarctic Climate and Ecosystems Cooperative Research Centre, University of Tasmania, Hobart, Tasmania, Australia
[2]Swiss Polar Institute, École Polytechnique Fédérale de Lausanne, Lausanne, Switzerland
[3]Commonwealth Scientific and Industrial Research Organisation Oceans and Atmospheres, Hobart, Tasmania, Australia
[4]Institute for Marine and Antarctic Studies, University of Tasmania, Hobart, Tasmania, Australia

Correspondence to: Christina Schallenberg (christina.schallenberg@utas.edu.au)
ORCID: 0000-0002-3073-7500

Abstract.

Evaluation of photosynthetic competency in time and space is critical for better estimates and models of oceanic primary productivity. This is especially true for areas where the lack of iron limits phytoplankton productivity, such as the Southern Ocean. Assessment of photosynthetic competency on large scales remains challenging, but phytoplankton chlorophyll-a fluorescence (ChlF) is a signal that holds promise in this respect as it is affected by, and consequently provides information about, the photosynthetic efficiency of the organism. A second process affecting the ChlF signal is heat dissipation of absorbed light energy, referred to as non-photochemical quenching (NPQ). NPQ is triggered when excess energy is absorbed; i.e., when more light is absorbed than can be used directly for photosynthetic carbon fixation. The effect of NPQ on the ChlF signal complicates its interpretation in terms of photosynthetic efficiency, and therefore most approaches relating ChlF parameters to photosynthetic efficiency seek to minimize the influence of NPQ by working under conditions of sub-saturating irradiance. Here, we propose that NPQ itself holds potential as an easily acquired optical signal indicative of phytoplankton physiological state with respect to iron (Fe) limitation.

We present data from a research voyage to the Subantarctic Zone south of Australia. Incubation experiments confirmed that resident phytoplankton were Fe-limited, as the maximum quantum yield of primary photochemistry, Fv/Fm, measured with a Fast Repetition Rate fluorometer (FRRf), increased significantly with Fe addition. The NPQ "capacity" of the phytoplankton also showed sensitivity to Fe addition, decreasing with increased Fe availability, confirming previous work. The fortuitous presence of a remnant warm-core eddy in the vicinity of the study area allowed comparison of fluorescence behaviour between two distinct water masses, with the colder water showing significantly lower Fv/Fm than the warmer eddy waters, suggesting a difference in Fe limitation status between the two water masses. Again, NPQ capacity measured with the FRRf mirrored the behaviour observed in Fv/Fm, decreasing as Fv/Fm increased in the warmer water mass. We also analysed the diel quenching of underway fluorescence measured with a standard fluorometer, such as is frequently used to monitor ambient chlorophyll-a concentrations, and found a significant difference in behaviour between the two water masses. This difference was quantified by defining an NPQ parameter akin to the Stern-Volmer parameterization of NPQ, exploiting the fluorescence quenching induced by diel fluctuations in incident irradiance. We propose that monitoring of this novel NPQ parameter may enable assessment of phytoplankton physiological status (related to Fe availability) based on measurements made with standard fluorometers, as ubiquitously used on moorings, ships, floats and gliders.

1. Introduction

A key limitation to confident estimates of global ocean productivity is the lack of readily obtained information regarding the physiological status of phytoplankton. Assessment of photosynthetic competency in time and space is a crucial requirement

for improved estimates and models of oceanic primary productivity. This is especially true for areas where iron (Fe) limitation is prevalent, such as the Southern Ocean (Boyd et al., 2007; Moore et al., 2013). Fe-induced variations in primary productivity in this region have been shown to arise from physiological drivers of photosynthesis that are currently poorly represented in models of productivity (Hiscock et al., 2008). The Southern Ocean is of particular interest because of its large influence on the global carbon cycle, which is directly linked to photosynthetic performance of the resident phytoplankton (Martínez-García et al., 2014; Sigman and Boyle, 2000). While photosynthetic performance can readily be measured on small scales, i.e. during ship-based surveys conducting incubations for estimates of primary productivity, assessment of photosynthetic competency on larger scales remains challenging. Fluorescence emitted by phytoplankton upon absorption of light is a signal that holds great promise in this respect, as it stems directly from the photosynthetic apparatus of phytoplankton and can be measured by instruments mounted on drifters, floats, gliders and even satellites (Letelier et al., 1997; Behrenfeld et al., 2009; Huot et al., 2013; Morrison, 2003; Schallenberg et al., 2008). Indeed, the signal has been shown to hold the potential for providing information on the physiological state of phytoplankton (Letelier et al., 1997; Behrenfeld et al., 2009; Morrison and Goodwin, 2010; Schallenberg et al., 2008).

Chlorophyll-a fluorescence (ChlF) is one of three pathways that light energy can take once absorbed by the light-harvesting antenna of photosystem II (PSII) of a photosynthetic organism. The other two possible pathways are photochemistry (i.e., primary charge separation in reaction center II (RCII)), and heat dissipation. Heat dissipation of absorbed light energy can be upregulated in situations where light energy is absorbed in excess of photosynthetic capacity, which has the potential to damage the photosynthetic apparatus. As the three possible pathways of absorbed energy are complementary, an upregulation of heat dissipation will quench the ChlF signal, which is known as non-photochemical quenching (NPQ) (Horton, Ruban, and Walters, 1996; Krause and Weis, 1984; Müller et al., 2001).

At midday, NPQ can depress the ChlF signal by up to 90% (Falkowski et al., 2017). This affects day-time ChlF data from ships, satellites, bio-optical floats and gliders, the latest and rapidly growing additions to the oceanographic toolbox (Biermann et al., 2015; Grenier et al., 2015; Xing et al., 2012; 2018). Sensitivity of NPQ to the light acclimation state of phytoplankton has been demonstrated (Milligan et al., 2012; O'Malley et al., 2014), and other drivers of NPQ, including nutrient status and species composition, have also been suggested (e.g., Kropuenske et al., 2009; Schallenberg et al., 2008; Schuback et al., 2015). An empirical relationship between sea surface temperature and NPQ in the Southern Ocean has been described (Browning et al., 2014), but the underlying controls are not fully understood.

Active fluorometers such as a Fast Repetition Rate fluorometer (FRRf) exploit the complementary nature of the three possible pathways of absorbed light energy. Triggering and detecting changes in ChlF in the dark-regulated state (i.e., when NPQ is relaxed and does not quench ChlF), allows derivation of the commonly used parameter Fv/Fm. Fv/Fm, often referred to as the maximum quantum yield of PSII, is a measure of the maximum fraction of absorbed light energy which can be used for primary charge separation in RCII. Strong links have been established between phytoplankton Fe status and Fv/Fm. As Fe becomes more and more limiting, Fv/Fm decreases (Geider et al., 1993; Greene et al., 1992). Benchtop FRRf instruments furthermore can quantify the induction of NPQ in response to increases in absorbed light energy, and recent studies have found a strong link between the capacity to induce NPQ and the Fe limitation status of phytoplankton (Alderkamp et al., 2012; Schuback et al., 2015; Schuback and Tortell, 2019).

The term "non-photochemical quenching" is a blanket term for a number of processes and parameterizations, with whole books dedicated to its many manifestations (e.g., Demmig-Adams et al., 2014). At its core, it is a photoprotective mechanism that safely removes excess excitation energy from the light harvesting system of photosynthesizers (Müller et al., 2001). It

can be assessed in many ways, the most clearly defined ones measured with active fluorometers such as FRRf, which allow measurements in both the dark- and light-regulated state. Common parameterizations of NPQ include the Stern-Volmer (SV) and Normalized Stern-Volmer (NSV) parameterizations, but a myriad of other definitions are in use (e.g., Rohacek, 2002). In a less strictly defined manner, NPQ can also be detected in measurements that are made with what we will call "standard

95 fluorometers" (SF) in this manuscript; i.e., fluorometers conventionally employed on floats, gliders, moorings, and ships to estimate ambient chlorophyll-a concentrations as a proxy for phytoplankton biomass (e.g., Roesler et al., 2017). Here, NPQ can take the form of depressed fluorescence in the middle of the day relative to the night, or it can manifest as a depression of fluorescence towards the ocean surface in daytime fluorescence profiles (Biermann et al., 2015; Grenier et al., 2015; Xing et al., 2012; 2018). Standard fluorometers are deployed ubiquitously in the oceans and can be operated remotely; the

100 prospect of harnessing physiological information contained in the NPQ signal they detect is thus tantalizing. Given the link between NPQ – as estimated with active fluorometers – and the Fe limitation status of phytoplankton (Alderkamp et al., 2012; Schuback et al., 2015; Schuback and Tortell, 2019), we investigated whether the NPQ signal detected by a standard fluorometer can also be interpreted with respect to the Fe limitation status of the resident phytoplankton community.

105 The two main objectives of this study were as follows: i) Link NPQ capacity as measured with a FRRf to NPQ measured with a standard fluorometer; ii) Link the NPQ signals from both to the Fe limitation status of the resident phytoplankton community. The first objective accounts for the fact that measurements with an FRRf are made under very controlled conditions, while the fluorescence detected with a standard fluorometer is measured under ambient conditions that can be highly variable due to differences in incident sunlight, in the rate of change in illumination (e.g., due to passing clouds), and

110 in the mixing depth, which also affects light history and acclimation. We further note that there is a ship-specific period of "dark-acclimation" prior to measurement if the standard fluorometer is installed on a ship's underway seawater line, yielding an acclimation status of the phytoplankton that is neither fully dark-regulated, nor fully light-regulated since some NPQ components can be reversed on the order of minutes and even seconds (Müller et al., 2001).

115 In order to investigate our research objectives, we undertook the following measurements and experiments on a voyage to the Subantarctic Zone (SAZ) south of Australia: 1) deckboard incubation experiments under controlled Fe conditions to confirm the link between Fe limitation and NPQ capacity, as measured with an FRRf, in the resident phytoplankton. 2) FRRf measurements on samples from the underway seawater line, yielding estimates of F_v/F_m and NPQ capacity that could be related to the Fe limitation status of the phytoplankton. This step revealed that two distinct water masses had been repeatedly

120 sampled by the ship, with significantly different F_v/F_m, indicating differences in their Fe limitation status. 3) NPQ estimated from the standard fluorometer on the underway seawater line was linked to the different water masses and thus to Fe limitation status, as well as to F_v/F_m and NPQ capacity measured with an FRRf.

2. Methods
125

2.1 Oceanographic setting and sampling
A research voyage to the Southern Ocean Time Series (SOTS) mooring site near 140°E and 47°S took place from March 3 to 20, 2018 aboard the *RV Investigator*. The SOTS site lies in the SAZ southwest of Tasmania, an area of considerable mesoscale and sub-mesoscale variability (Shadwick et al., 2015; Weeding and Trull, 2014). During occupation of the area, a

130 remnant eddy with sea surface temperatures (SST) >14°C was just east of the SOTS site and was visited multiple times by the ship (Fig. 1).

3

The ship's underway seawater supply, which had an intake in the ship's drop keel (water depth ~7 m), was equipped with a WETStar fluorometer (Wetlabs, Inc., Philomath, Oregon, USA) that measured ChlF at 695 nm (excitation at 460 nm) continuously throughout the voyage. Travel time through the ship's plumbing from intake to the fluorometer was between 1 and 2 minutes. The underway seawater line also supplied water to a WETLabs absorption and attenuation meter (ac-9) in flow-through mode (see below). At regular intervals, the underway seawater supply was sampled for pigment analysis by high performance liquid chromatography (HPLC), particulate absorption spectra following the filter pad approach (Mitchell, 1990), and chlorophyll-a concentration analysed fluorometrically (Chl-a), ; more details on the respective methods below)and for fluorescence light curves measured with an FRRf (more details on the respective methods below). Oceanic profiles (conductivity, temperature, depth, hereafter CTD) were collected at 6 stations using Sea-Bird SBE 9*plus* instrumentation, with associated sampling conducted from a 36-bottle rosette equipped with 12 L Niskin bottles. Onboard measurements of oxygen and salinity on discrete samples from the Niskin bottles were used to calibrate CTD sensors. Samples for macronutrients (NO_x (sum of nitrate and nitrite), sSilicate, pPhosphate) were also drawn from Niskin bottles and analysed onboard with a Seal AA3 segmented flow instrument following the methods of Rees et al. (2019).

2.2 Incubation experiments

At 3 stations, all located in close vicinity to 47°S, 142°E, either a trace metal clean rosette system (TMR) or a trace metal clean pumped "fish" (i.e., a submerged body towed from abeam and outside the ship wake with an intake at 3-5 m depth) were deployed in order to retrieve uncontaminated samples uncontaminated by trace metals. For each of the 3 incubation experiments, one initial HPLC sample was drawn, and 4 acid-washed polycarbonate bottles (250 mL each) were filled with unfiltered seawater from the mixed layer and incubated in a deck incubator that was continuously supplied with surface seawater for temperature control. Light levels were controlled with mesh bags placed around the bottles (see Table 1). Each experiment consisted of the following 4 treatments (final concentrations indicated):

- 20 nM desferrioxamine B (DFB), a strong iron chelator
- Control (no additions)
- 0.2 nM Fe (added as $FeCl_3$ dissolved in acidified Milli-Q water)
- 2 nM Fe (added as $FeCl_3$ dissolved in acidified Milli-Q water)

Incubations were run for ~51.5-55 hours (see Table 1), and at the end of the experiments each polycarbonate bottle was sub-sampled for an FRRf measurement (see below). Fluorescence parameters are sensitive to the light history experienced by the phytoplankton, so the time of day at which measurements are made can change results. In order to make all 4 treatments comparable to each other, they had to be measured as closely in time as possible, hence only one replicate per treatment was prepared, allowing us to complete one round of FRRf measurements in less than 2 hours. The duration of the incubations was chosen to allow an adequate physiological response time (see Fig. S1 in the Supplementary Information for the time course of experiment 1, indicating that results were consistent between 29 h and 52 h sampling points, but more pronounced after 52 h).

2.3 Photosynthetic competency: FRRf measurements

Photosystem II (PSII) variable ChlF was measured on a Fast Repetition Rate fluorometer (FRRf, Chelsea Technologies Group FastOcean Sensor fitted with an Act2 laboratory system) using the factory-supplied Act2Run software. All measurements were made in a temperature-controlled room that was kept at the ambient SST temperature (10-14°C). Prior to each measurement, a blank was prepared by filtering a small aliquot of sample through a 0.2 μm syringe filter, and was subsequently subtracted from all measured fluorescence signals. The excitation wavelength of the FRRf's light-emitting diodes (LEDs) was 450 nm, and the instrument was used in single turnover mode, with a saturation phase comprising 100 flashlets on a 2 μs pitch and a relaxation phase comprising 40 flashlets on a 60 μs pitch. Samples were low-light acclimated

4

(at 2-5 µmol quanta m^{-2} s^{-1}) for ~1 h prior to each fluorescence light curve measurement to ensure ~~complete~~ relaxation of ~~all~~ fast-relaxing NPQ as well as some (but likely not all) slow-relaxing NPQ. Measurement of each fluorescence light curve took 24 min and comprised 8 light steps of increasing intensity (see Fig. S2 in SI for details)~~, with the majority of light steps lasting 30 seconds except for the following: darkness (300 seconds), the final, highest light step (600 seconds), the previous light step (300 seconds) and the light step before that (120 seconds). These durations were chosen to "gently" induce NPQ at high light.~~ Fluorescence light curves were optimized to yield estimates of NPQ capacity ~~(details below)~~ at light intensities of either 750 µmol quanta m^{-2} s^{-1} (for samples from the underway seawater system) or 1000 µmol quanta m^{-2} s^{-1} (incubation samples). These high-light intensities were chosen based on experimentation earlier in the voyage and represent a balance such that a curve could still be fitted to the fluorescence induction data, while maximizing the NPQ signal. Since maximum NPQ capacity was our main focus, we chose an experimental design that struck a balance between i) ensuring a good fit at the maximum light intensity, ii) increasing light levels slowly enough to allow the cells to ~~keep up~~ reach steady-state quenching (thus choosing longer time steps at the more stressful high light intensities), and iii) keeping the fluorescence light curves as short as possible so that the four treatments in each incubation experiment could be measured within the smallest time frame possible (<2h) in recognition of the sensitivity of fluorescence parameters to light history and time of day.

Three measured fluorescence signals, F_o, F_m and F_m' were used to calculate fluorescence parameters, following Rohacek (2002). F_o and F_m refer to minimum and maximum fluorescence in the dark-acclimated state, while F_m' is the maximum fluorescence in the light-regulated state, in this case measured at the highest light level of the respective fluorescence light curve.

The maximum quantum yield of PSII, Fv/Fm, was estimated from fluorescence measurements during the dark step of the fluorescence light curve as follows:

$$\frac{F_v}{F_m} = \frac{F_m - F_o}{F_m} \qquad (1)$$

There are a number of different NPQ formulations available in the literature (e.g., see Rohacek, 2002), with their respective advantages and disadvantages. We chose to focus on two parameterizations: Stern-Volmer (NPQ$_{SV}$) and the normalized Stern-Volmer NPQ (NPQ$_{NSV}$):

$$NPQ_{SV} = \frac{F_m - F_m'}{F_m'} \qquad (2)$$

$$NPQ_{NSV} = \frac{F_o'}{F_v'} \qquad (3)$$

with F_o' calculated following Oxborough and Baker (1997): $\quad F_o' = \frac{F_o}{\left(\frac{F_v}{F_m} + \frac{F_o}{F_m'}\right)} \qquad (4)$

and $\qquad F_v' = F_m' - F_o' \qquad (5)$

Both parameters were estimated at the respective maximum light levels of the fluorescence light curves (i.e., 750 and 1000 µmol quanta m^{-2} s^{-1} for underway and incubation samples, respectively) and should thus be regarded as a NPQ "capacity" which can be achieved under given nutrient availabilities and light histories of the phytoplankton assemblage (*c.f.* Schuback and Tortell, 2019). The light levels at which the NPQ parameters were measured are indicated in parentheses in the respective Figures; see also Table 2 for a summary of fluorescence parameters discussed in this paper.

2.4 Phytoplankton pigments and absorption

2.4.1 HPLC analyses
220 Sample volumes of 3-4 litres were filtered through a 25 mm glass fibre filter (Whatman GF/F), blotted dry and stored at – 80 °C until analysis. Samples were extracted over 15–18 hours in an acetone solution before analysis by high performance liquid chromatography (HPLC) using a C_8 column and binary gradient system with an elevated column temperature following the method of Clementson (2013). Pigments were identified by retention time and absorption spectrum from a

225 photo-diode array (PDA) detector, and concentrations of pigments were determined from commercial and international standards (Sigma, USA; DHI, Denmark).

2.4.2 Diagnostic pigment indices
The results from HPLC analyses were used to derive diagnostic pigment (DP) indices following Barlow et al. (2008), which
230 give an indication of the phytoplankton community composition in terms of three functional groups: diatoms, flagellates and prokaryotes. The DP index and resulting functional groups are defined based on 7 biomarker pigments as follows:

DP = (alloxanthin (Allo) + 19'-hexanoyloxyfucoxanthin (Hex-fuco) + 19'-butanoyloxyfucoxanthin (But-fuco) + fucoxanthin (Fuco) + zeaxanthin (Zea) + chlorophyll b (Chl-b) + peridinin (Perid))

Diatoms = Fuco/DP
235 Flagellates = (Allo + Hex-fuco + But-fuco + Chl-b)/DP

Prokaryotes = Zea/DP

2.4.3 Fluorometric measurement of chlorophyll
Samples for fluorometric Chl-a analyses (2 L) were filtered onto 25 mm glass fibre filters (Whatman, GF/F) and
240 immediately frozen at –80 °C. Within 3 weeks of sampling, all filters were extracted with 10 mL of 90 % acetone at –20 °C for 24 hours. Fluorescence was measured on a Turner Trilogy Laboratory Fluorometer and converted to Chl-a following the acid ratio method (Holm-Hansen et al., 1965). The fluorometer using had been a standard chlorophyll-a dilution that was calibrated with a spectrophotometrically measured dilution series with a standard chlorophyll a dilution (Jeffrey and Humphrey, 1975).

245

Fluorometric Chl-a showed excellent agreement with Chl-a measured using the HPLC method, albeit with an offset and a slight decrease in the slope relative to the 1:1 line (Fig. S31 in SI). In order to bring the Chl-a measured fluorometrically in line with the more precise HPLC measurement (e.g., Trees et al. 1985), all fluorometric Chl-a estimates were corrected using the slope and intercept from the regression of HPLC Chl-a against fluorometric Chl-a ($Chl_{HPLC} = Chl_F * 0.879 - 0.052$; $r^2 =$
250 0.97, n = 15, standard error of the estimate = 0.029 mg m^{-3}). All Chl-a estimates could thus be combined for calibration of the ac-9 absorption line height approach (see below).

2.4.4 Phytoplankton absorption (filter pad):
Sample volumes of 3–4 litres were filtered through a 25 mm glass fibre filter (Whatman GF/F), and the filter was then stored
255 flat at –80°C until analysis. Optical density spectra for total particulate matter were obtained using a Cintra 404 UV/VIS dual beam spectrophotometer equipped with an integrating sphere. Quartz glass plates were used to hold the sample and blank filters against the integrating sphere. The optical density of the total particulate matter of each sample was obtained using a blank filter as a reference (from the same batch number as the sample filters) wetted with filtered seawater (0.2 µm) and scanned from 200–900 nm with a spectral resolution of 1.3 nm. Following the scan for total particulate matter, the sample

260 filter was returned to the original filtering units, and any pigmented material was extracted using the method of Kishino et al. (1985). Blank reference filters were treated in the same manner. The filters were rinsed with filtered seawater and then rescanned to determine the optical density of the detrital or non-algal matter. An estimate of the optical density due to phytoplankton was obtained as the difference between the optical density of the total particulate matter and the detrital or non-algal matter. The optical density scans were converted to absorption spectra by first normalizing the scans to zero at 750

265 nm and then correcting for the path length amplification using the coefficients of Mitchell (1990).

2.4.5 Particulate absorption (ac-9):

A WETLabs ac-9 instrument with 25-cm flow tubes was employed in underway mode on the underway seawater line of the *RV Investigator*. The instrument was immersed in the upright position in a flow-through water bath for temperature control,

270 and the flow tubes were shielded from ambient light. Flow was upwards through the tubes and trickled from there into the water bath, where an overflow valve controlled the water level. About 2/3 of the instrument was immersed, with the upper part exposed to the atmosphere. Internal instrument temperature was monitored every few hours and fluctuated between 21 and 26°C. The inflow was manually switched between unfiltered and filtered seawater (0.8/0.2 μm; AcroPak^{TM} 1500 capsule filter with Supor® membrane), with filtered measurements lasting ~10 min and conducted every ~2 h. The fFlow rate was 1–

275 1.5 L min^{-1} for unfiltered seawater and not lower than 0.5 L min^{-1} for filtered seawater. The filter was exchanged for a new one after 10 days.

Because we were interested only in the absorption line height at 676 nm, only the red absorption channels of the ac-9 (λ = 650, 676 and 715 nm) were processed. Analysis of repeat measurements on Milli-Q water in the laboratory prior to the

280 voyage (2–7 minutes each, then the average taken for each measurement) indicated that the precision of these 3 channels ranged 0.0023 – 0.0028 m^{-1} (2.3–2.9 %) when expressed in terms of the standard deviation of measurements (n=8). The absolute range, determined as the difference between the maximum and minimum value of the measurements, was 0.0059 – 0.0071 m^{-1} (5.9–7.4 %).

285 Bubbles in the flow tubes were a common problem on the voyage and were dealt with by applying a thorough cleaning routine as well as smoothing of the time series during processing (see SI for details). Particulate absorption was calculated by subtracting interpolated filtered measurements (i.e., dissolved absorption) from unfiltered measurements (total absorption) at each wavelength (Slade et al., 2010). The particulate absorption line height at 676 nm (LH(676), m^{-1}) was then calculated following Roesler and Barnard (2013), subtracting a baseline based on absorption measurements at 650 and 715

290 nm. This LH(676) was calibrated against discrete Chl-a (Chl-a from fluorometric and HPLC measurements combined, see above) and also against phytoplankton absorption as determined with the filter pad method (see SI).

2.5 Simulated *in situ* measurements of size fractionated primary production

Photosynthetic production of organic matter was measured twice during the voyage (7 March and 18 March, 2018; both

295 times with water from SST <11.5°C) by the 14-Carbon (^{14}C) tracer method. Algal carbon fixation was measured on samples collected pre-dawn from trace metal clean Niskin bottles deployed on a TMR from 3 or 4 depths: 35, 50, (70 m for the 18 March incubation) and 100 m. Sampling depths were determined from *in situ* irradiance depth profiles obtained during midday CTD casts the day prior to collection. Samples were dispensed into 300 mL acid-washed polycarbonate bottles and spiked with 16 μCi of Sodium ^{14}C-bicarbonate (NaH^{14}CO$_3$; specific activity 1.85 GBq mmol^{-1}; PerkinElmer). Following the

300 addition of ^{14}C, samples were incubated for 24 h in neutral density mesh bags in a deckboard incubator. The temperature of the incubator was controlled by a continuous supply of surface seawater. Six samples (5 light and one dark bottle per irradiance) were incubated under natural sunlight at 6 light intensities (from 67 to 0.2 % of incident irradiance), which were

Formatted: Superscript

adjusted by varying the layers of neutral density mesh. Light attenuation was measured with a Biospherical Instruments QSL2101 Quantum Scalar PAR (Photosynthetically Available Radiation) Sensor. Carbon fixation based on radioisotope measurements and 24-hour incubations are reported to approximate net primary production (Laws, 1991).

Upon completion of the 24-h incubation, 4 replicate samples were filtered in series through 0.2, 2.0, and 20 µm polycarbonate filters (Poretics) separated by 200 µm nylon mesh, and two samples were filtered through 0.2 µm filters (a total community 'light' control, and a total community 'dark' control). Data for the dark-corrected size-fractionated samples are reported here. Filters were rinsed with 0.2 µm-filtered seawater, acidified to volatilize any remaining inorganic carbon (Boyd and Harrison, 1999), and collected in 20 mL glass scintillation vials (Wheaton) to which 10 mL of liquid scintillation cocktail (UltimaGold, PerkinElmer) was added. Samples were subsequently analysed by liquid scintillation counting (PerkinElmer Tri-Carb 2910 TR). Water column integrated carbon assimilation rates were calculated using the trapezoid rule with the shallowest value extended to 0 m and the deepest extrapolated to a value of zero at 200 m.

2.6 Mooring data

We show SOTS mooring data from the Pulse-7 deployment in 2010-2011. The mooring was equipped with a number of instruments including a downward-looking WETLabs ECO FLNTUS fluorometer with a "bio-wiper" at 30 m and a wiped ECO PAR (photosynthetically available radiation) sensor at the same depth. Seawater temperature was measured at 15 discrete depths with Vemco Minilog Classic sensors (except for the shallowest sensor at 30 m, which was a SeaBird Electronics SBE16plusV2), and mixed layer depth (MLD) was calculated based on a temperature difference of 0.3°C relative to the 30 m measurement. Only data with a quality flag <2 were used, and the fluorescence sensor had been calibrated using factory-supplied dark values and scale factors (Schallenberg et al., 2019). Fluorescence-based WETLabs ECO sensors have been shown to overestimate Chl-a in the Southern Ocean by up to a factor of 7 compared to pigment samples, with a factor of ~4 overestimation reported for the South Indian Ocean (Roesler et al., 2017). We have thus divided the fluorescence output from the FLNTUS sensor by 4 when Chl-a concentration as a proxy of phytoplankton biomass was the entity of interest, consistent with previous approaches to fluorescence data from the SAZ (e.g., Eriksen et al., 2018). However, the fluorescence data were also used to estimate NPQ over the daily cycle, and for this exercise fluorescence was not divided by 4, nor was it in any other way normalised to biomass.

NPQ from the FLNTUS fluorometer was estimated analogously to the Stern-Volmer parameterization

$$NPQ_{SF} = \frac{F_{max} - F_{min}}{F_{min}} \qquad (6)$$

where NPQ_{SF} stands for NPQ measured with a standard fluorometer and F_{max} and F_{min} are the maximum and minimum fluorescence measurements made with said fluorometer in a day, with the following restrictions: the daily fluorescence and PAR data were first smoothed with a Loess filter, and NPQ_{SF} was only estimated if the minimum fluorescence was within 2 hours of maximum PAR. The parameter F_{max} designates the maximum smoothed fluorescence between 5 am and noon on a given day. This was preferable to using F_{max} from night-time because it provides that the two fluorescence measurements are closer in time, and thus the likelihood of F_{max} varying due to fluctuations in Chl-a concentrations is reduced. Furthermore, this approach corresponds to analyses carried out on the underway fluorescence data from the SOTS voyage, discussed below. Note that NPQ_{SF} is a "realized" NPQ at incident light, in contrast to the NPQ "capacity" estimated with the FRRf.

3. Results and Discussion

3.1 Incubation experiments: sensitivity of ChlF parameters to Fe status

8

345 The incubation experiments were designed with the goals to: 1) test whether the resident phytoplankton were Fe-limited and
2) investigate how NPQ capacity and Fv/Fm, as derived from FRRf measurements, respond to changes in ~~iron~~ Fe status. All
3 incubations were carried out with source waters colder than 11.5°C (Table 1); i.e., with waters from the colder water mass
as evident in Fig. 1, and the respective pigment compositions of the resident phytoplankton were very similar (Fig. S4~~2~~),
indicating a dominance of haptophytes, with some diatoms and chrysophytes also present. The pooled data from the
350 experiments show unequivocally that Fe addition increased the maximum quantum yield of PSII, Fv/Fm, as has been
observed previously in HNLC regions (e.g., Boyd and Abraham, 2001; Kolber et al., 1994). The NPQ capacity, measured as
both $NPQ_{SV}(1000)$ and $NPQ_{NSV}(1000)$, decreased with ~~iron~~ Fe addition (Fig. 2), most likely due to increased capacity to use
absorbed light energy for photochemistry. The functional absorption cross section of PSII, σ_{PSII}, also decreased with Fe
addition, as has been observed previously (Kolber et al., 1994; Schuback et al., 2015; Schuback and Tortell, 2019). Overall,
355 σ_{PSII} were very large in all treatments (~10–12 nm^2 RC^{-1}), as has been observed previously for low Fe-adapted Southern
Ocean phytoplankton (Strzepek et al., 2012; Strzepek et al., 2019). The addition of DFB, a strong organic ligand
(siderophore) that decreases Fe availability to phytoplankton, had the opposite effect to Fe addition for all parameters. The
phytoplankton thus showed a clear response to changes in Fe status, which affected their ability to process absorbed light
energy, evident in a lower maximum quantum yield of PSII, Fv/Fm, and an increased capacity and need to dissipate excess
360 excitation energy as NPQ.

For all parameters except σ_{PSII}, the results for the +Fe treatment were significantly different from the respective control
(Wilcoxon rank sum test, $p < 0.05$), indicating that phytoplankton in the sampled water mass, i.e. the cold waters <11.5°C,
were Fe-limited. This view is further supported by the low initial Fv/Fm observed for all experiments (~0.33, Table 1); a
365 fully dark-regulated Fv/Fm in this range is a widely accepted indicator of Fe limitation in HNLC waters (Boyd and
Abraham, 2001; Kolber et al., 1994; Suggett et al., 2009).

The changes in NPQ capacity were diametrically opposite to the changes in Fv/Fm with respect to Fe status: as Fe stress
increased, so did the capacity for NPQ. Similar NPQ responses to Fe status have been observed previously in controlled
370 experiments both in the laboratory and with natural phytoplankton communities from Fe-limited ocean regions (e.g.,
Alderkamp et al., 2012; Petrou et al., 2014; Schuback et al., 2015; Schuback and Tortell, 2019). While some of these studies
reported NPQ_{SV}, others estimated NPQ_{NSV}, hence we decided to investigate the Fe-effect on both. Non-photochemical
quenching affects all fluorescence levels and is easiest quantified using the Stern-Volmer parameterization, which was
originally developed for higher plants. However, this parameterization does not take into account differences in Fv/Fm in the
375 dark-regulated state, which can mask differences in NPQ as only the light-induced component is assessed, ignoring
differences in basal levels of heat dissipation. The Normalized Stern-Volmer parameterization explicitly accounts for
differences in Fv/Fm, which means it is a more appropriate parameter when samples with different Fv/Fm are being
compared, as is the case in our incubations with different levels of Fe stress. However, it is important to note that
mathematically, NPQ_{NSV} is inversely related to Fv/Fm when F_o' is calculated (see Eq 4) rather than measured directly, as is
380 the case in our study:

$$NPQ_{NSV} = \frac{\frac{F_o}{F_m'}}{\frac{F_v}{F_m}} \qquad\qquad (7)$$

This inverse mathematical relationship, in conjunction with the established sensitivity of Fv/Fm to Fe limitation (Boyd and
Abraham, 2001; Kolber et al., 1994; Suggett et al., 2009), means that NPQ_{NSV} is not a truly independent parameter with
respect to Fe status, even though the inverse relationship with Fv/Fm may be physiologically relevant. Furthermore,
385 measurement of NPQ_{NSV} requires knowledge or calculation of F_o or F_o' (Eq. 3-5), which means it can only be measured with

9

an active fluorometer, such as a FRRf. Conversely, parameters analogous to the NPQ_{SV} parameter can be estimated with any fluorometer so long as a dark-regulated and light-regulated measurement is available.

A physiological relationship between NPQ and Fe stress can be understood conceptually as a result of increased excitation
390 pressure on the reaction centres when Fe is limiting (Schuback et al., 2015). Under Fe stress, there are fewer reaction centres and electron transport chains per chlorophyll because electron transport chains are Fe-expensive (Behrenfeld and Milligan, 2013). More energy is thus funnelled to fewer reaction centres, which causes the increase in σ_{PSII} (Alderkamp et al., 2019; Ryan-Keogh et al., 2017; Strzepek et al., 2012). This arrangement comes at the expense of the ability to deal with fluctuations in light; the system is "less robust". Iron limitation thus increases the need for rapid photoprotection, which can
395 be achieved through an increased capacity for NPQ, as has been observed previously (Schuback et al., 2015, Schuback and Tortell, 2019).

From the data presented above, we conclude that the resident phytoplankton in the colder water mass were indeed Fe-limited (evident in the clear treatment response to Fe-addition, Fig. 2), and that both the NPQ capacity and Fv/Fm, as derived from
400 FRRf measurements, responded to changes in Fe status. While Fv/Fm increased with Fe addition, the NPQ capacity decreased, consistent with expectations. The observation that the colder water mass exhibited signs of Fe-limitation is also consistent with expectations, as the SAZ, and in particular the SOTS site, has been shown to be seasonally Fe-limited, with limitation increasing towards the end of summer (Boyd et al., 2001; Hutchins et al., 2001; Lannuzel et al., 2011; Sedwick et al., 1999).
405

3.2 Underway data: two SST regimes with different ChlF parameters (FRRf)
Fluorescence measurements similar to the ones carried out on the incubations were also performed on samples taken from the underway seawater line on the SOTS voyage (n=66). Fv/Fm ranged from 0.2 to 0.5 in the resident phytoplankton and showed an inverse relationship with NPQ capacity (Fig. 3), as was observed for the incubations. The trends in ChlF
410 parameters appeared to fall into two groups based on sea surface temperature (SST): phytoplankton in the colder water mass (<11.5°C) showed lower Fv/Fm and higher NPQ capacity, consistent with increased Fe limitation, compared to the phytoplankton in the warmer water mass (>13.5°C). Grouping the ChlF parameters based on SST illustrates this point even further (Fig. 4): Fv/Fm, as well as the capacity to dissipate excess excitation energy (estimated as NPQ_{NSV} and NPQ_{SV}), were significantly different between the two water masses ($p \ll 0.01$, Wilcoxon rank sum test). It thus appears that the
415 phytoplankton in the two SST regimes experienced different levels of Fe stress, but before such a conclusion can be drawn, a number of confounding factors must be discussed, including species composition, mixed layer depth, and the effect of temperature on physiology.

3.2.1 Phytoplankton pigments and community composition in the two SST regimes
420 The diagnostic pigment (DP) index, calculated from HPLC pigment analyses, provides a simple though not definitive means to investigate phytoplankton community composition. It focusses on three major groups (diatoms, flagellates and cyanobacteria) selected on the basis of their significance rather than their respective size ranges (Barlow et al., 2008). Such a diagnostic index is naturally a simplification and should be treated with caution. However, the DP index has been used across a number of ecological ocean regions, including the SAZ and Southern Ocean, where it compared favourably to the
425 more elaborate CHEMTAX analyses (e.g., Mendes et al., 2015).

Our analysis indicates a dominance of flagellates in both the warm and cold SST regimes, with diatoms and prokaryotes playing a lesser role (Fig. 5). Despite some differences between the two SST regimes, the overall pattern is similar,

indicating that the phytoplankton assemblages in the two water masses were comparable (see Fig. S5~~3~~ and S6~~4~~ for detailed

430 pigment and phytoplankton absorption results). Moreover, these distributions among major phytoplankton groups are consistent with the phytoplankton community composition in the SAZ reported by Mendes et al. (2015) using similar methods. These authors also conducted a CHEMTAX analysis of their data that suggested a dominance of haptophytes in the SAZ, with pelagophytes, prasinophytes and diatoms making up the majority of other taxa. A recent microscopic analysis of fortnightly samples from a remote sampler on the SOTS mooring at 142°E, 47°S likewise indicated that flagellates were the

435 most abundant phytoplankton group between September and April, followed by diatoms (Eriksen et al., 2018). The results from the DP index analysis are thus consistent with previous estimates for the region and show that the two SST regimes were broadly similar with respect to phytoplankton community composition.

3.2.2 Mixed layer depths and average light field

440 The depth of the mixed layer can have a profound impact on NPQ capacity, as phytoplankton acclimate to their light exposure. Deeper mixed layers, resulting in stronger fluctuations in light availability, have been found to increase the NPQ capacity of phytoplankton in the field and under simulated conditions in the laboratory (Browning et al., 2014; Milligan et al., 2012). In our study region, the mixed layer depth was deepest in the warm SST regime (~100 m; Fig. S7~~5~~), while it ranged between 20 and 90 m in the colder regime~~.~~. The corresponding median daily integrated PAR in the mixed layer (for a

445 nominal clear-sky day in March and with PAR attenuation estimated as a function of Chl-a based on Morel et al., 2007) was 0.13 mol m^{-2} d^{-1} for the warm SST regime, while it ranged from 0.5 to 15 mol m^{-2} d^{-1} for the cold SST regime. ~~-~~If the ~~strength of~~ rates and magnitude of light intensity fluctuations ~~in light intensity~~ ~~mixed layer depth~~ were the driver~~s~~ for the observed differences in NPQ capacity between the two water masses, we would expect ~~that~~ the warmer water mass (with the deep mixed layer) to show increased NPQ capacity. However, the observed NPQ trend is exactly opposite, with higher NPQ

450 capacity evident in the colder water mass. With only one CTD station in the warmer SST regime, we may have under-sampled this water mass, but it is unlikely that it showed overall shallower mixed layers than the cold-water regime. We thus conclude that the observed trend in NPQ capacity can not be explained by the mixed layer depths encountered.

3.2.3 Temperature effects on phytoplankton photophysiology

455 It is well established that temperature has a strong effect on phytoplankton growth, especially with respect to the optimal niche for a given species (e.g., Boyd et al., 2013; Davison, 1991; Raven and Geider, 1988). However, the maximum quantum yield of PSII, Fv/Fm, appears less sensitive to temperature. Manipulative studies have reported little or no effect on Fv/Fm for phytoplankton grown at temperatures differing by 4–8°C between minimum and maximum temperature (e.g., Kulk et al., 2012; Rose et al., 2009). Indeed, the latter study specifically investigated the synergistic effects of Fe and

460 temperature on Antarctic phytoplankton. An increase in temperature by 4°C did not result in any change of Fv/Fm compared to the control, but an addition of Fe increased Fv/Fm significantly – with and without an increase in temperature (Rose et al., 2009). We thus conclude that it is highly likely that the differences in Fv/Fm and NPQ capacity we observed between the two SST regimes (with mean SSTs of 10.8±0.5°C and 14.6±0.7°C, respectively), were the result of physiological changes in the phytoplankton due to their nutritional (Fe) status, rather than being caused by the different ambient temperatures.

465

3.2.4 The case for differences in physiological status in the two SST regimes

The strongest indicator that the two SST regimes held phytoplankton communities with different levels of Fe stress is the difference in Fv/Fm between the two regimes (Fig. 4). The decrease in Fv/Fm in the colder water mass corresponded to a large increase in F_o relative to the warm regime (Fig. S8~~6~~), in line with the hypothesis that under Fe limitation damaged

470 and/or disconnected light harvesting complexes contribute to background fluorescence, as has been previously observed

(Behrenfeld and Milligan, 2013). The corresponding increase in F_m in the presumably Fe-limited water mass is also not unexpected and has been observed in other Fe-limited regions (e.g., Behrenfeld and Kolber, 1999).

Rates of water column integrated net primary productivity measured in the cold SST regime also point to Fe limitation in that water mass. Column integrated primary production rates ranged from 317 ± 30 mg C m^{-2} d^{-1} (18 March 2018) to 500 ± 104 mg C m^{-2} d^{-1} (7 March 2018). These rates agree well with those measured at the SOTS site in March 2016 using the same method (670 ± 25 mg C m^{-2} d^{-1}) (Ellwood et al., submitted), but are considerably lower than those measured by Westwood et al. (2011) in Ssubantarctic waters in austral summer (January-February 2007) when Fe concentrations are higher: 1034-1627 mg C m^{-2} d^{-1}. While part of the difference between our results and those of Westwood et al. (2011) may be due to methodological differences (i.e., short (2h) versus long (24h) ^{14}C incubations), we ascribe most of the difference to the seasonal cycle of Fe limitation observed previously for SOTS (Boyd et al., 2001; Hutchins et al., 2001; Lannuzel et al., 2011; Sedwick et al., 1999). See SI for a full comparison of observed conditions between this study and Westwood et al. (2011).

Fewer ancillary data are available for the warmer water mass, as there were no primary productivity measurements or Fe-addition experiments undertaken. However, macronutrient data from the one CTD in that water mass indicate that the warm SST regime was not High Nutrient, Low Chlorophyll (HNLC), as NOx was drawn down to near-zero, which was not the case for the colder waters where NOx was always well above 5 μMmol L^{-1} (Fig. S97). Phosphate concentrations were also significantly lower in the warmer waters than the cold waters, while silicate was depleted for both.

The SST map in Fig. 1 indicates that the warm SST signature near SOTS was part of a cyclonic eddy, which could be tracked back in time to even warmer waters south-west of Tasmania based on its signature on satellite altimetry and SST images (not shown). At the time of sampling, the eddy-associated water mass exhibited SSTs reaching >14°C, compared to <12°C for the waters further west, and it showed warmer and saltier water throughout the water column, with a salinity minimum around 34.4 (Fig. S108). Such a T-S signature is consistent with an origin of the eddy-associated water mass either east or west of Tasmania, with a strong influence from the Tasman Sea (Herraiz-Borreguero and Rintoul, 2011). Waters east of Tasmania have previously been found to be Fe-replete (and low in nitrate), with airborne dust and shelf sediments presumed to be the main Fe sources (Bowie et al., 2009; Lannuzel et al., 2011). Fv/Fm values indicative of Fe sufficiency (~0.5) were also reported for the SAZ south-east of Tasmania (SST ~15°C) in late summer, along with very low nitrate and non-limiting Fe concentrations at the surface (Hassler et al., 2014). It is thus highly likely that the warmer water mass encountered during the SOTS voyage in 2018 was Fe-replete, while the colder water mass was Fe-limited. The absence of dissolved Fe data leaves the Fe nutritional status of the warmer water mass community less than completely clear (although the presence of Fv/Fm values above 0.4 suggests Fe limitation was unlikely since Fe status is known to be the dominant driver for Fv/Fm in the Southern Ocean, e.g., Suggett et al. (2009)). Regardless of this uncertainty, the Fe-limited status and corresponding high NPQ capacity of the cold-water community is clear.

3.3 Underway data: Continuous measurements across the two SST regimes

The two SST regimes were repeatedly visited by the ship during the voyage (Fig. 6). The Chl-a data from the ac-9 were remarkably different from the fluorometer traces (compare Fig. 6b) and 6c)), with clear day-night fluctuations in the latter that were not reflected in the ac-9 data. These fluctuations were especially pronounced in the colder water mass, which had overall lower Chl-a concentrations than the warmer waters (mean Chl-a = 0.38 ± 0.06 mg m^{-3} for SST<11.5°C and 0.62 ± 0.11 mg m^{-3} for SST>13.5°C). The daily fluorescence minima coincided with the maxima in above-water incident

~~photosynthetically available radiation~~ (PAR~~)~~ and vice versa: i.e., fluorescence was highest during the night. Such daily fluorescence cycles are consistent with non-photochemical quenching of fluorescence in the daytime.

515

3.3.1 Physiological information in underway fluorescence: NPQ differences between the two SST regimes

In order to investigate NPQ as measured with the standard fluorometer (Fig. 6c) in more detail, we normalized fluorescence by Chl-a as estimated by the ac-9 and plotted it against incident daytime PAR (Fig. 7). Colour-coding by SST clearly shows that two NPQ regimes were at play. In the colder waters, F/Chl-a was high at low PAR and decreased considerably as PAR
520 increased – dynamic NPQ was high. In the warmer waters, F/Chl-a was relatively constant across PAR values and dynamic NPQ was thus low. Note that normalization to Chl-a removes differences in the fluorescence signal that would be caused by differing Chl-a concentrations in the water masses.

The NPQ signal from the standard fluorometer was further investigated by formally separating the data from the two water
525 masses based on SST (Fig. 8). A Loess filter was applied to the respective pooled data sets (for values measured at PAR>5 and PAR<1000 μmol quanta m^{-2} s^{-1}), and NPQ$_{SF}$ ("NPQ measured with a standard fluorometer") was estimated from the filtered data according to Eq (6). The NPQ$_{SF}$ signal in the colder, HNLC water mass was more than twice as high as that in the warm SST regime, and a similar trend was discernible even without normalization of the fluorescence signal to Chl-a (Fig. 8). The trends in NPQ as evidenced in the data from the standard fluorometer are thus consistent with the NPQ
530 capacities measured with the FRRf (Fig. 4): increased dynamic NPQ (and NPQ capacity) in the colder waters relative to the warm SST regime. This result is significant for it indicates that measurements from a standard fluorometer can be interpreted with regards to phytoplankton physiological status. Without the control afforded by an FRRf, simply with a standard fluorometer and the daily cycle of the sun, a signal is measured (NPQ$_{SF}$) that holds profound physiological information. This shouldn't come as a complete surprise, as it has long been recognized that standard fluorometers are affected by NPQ, and
535 considerable research has gone into investigating how to best correct for NPQ in order to retrieve more accurate profiles of Chl-a concentration (Biermann et al., 2015; Thomalla et al., 2018; Xing et al., 2012, 2018). However, given the dependence of NPQ on incident irradiance, attempts to correct for it in a "physiological" way have tended to be based on irradiance thresholds or light history (e.g., Behrenfeld et al., 2009; Xing et al., 2018), while ignoring other factors affecting phytoplankton physiological status, such as Fe limitation.

540

A noteworthy exemption is the study by Browning et al. (2014), which specifically investigated the variability of NPQ along eco-physiological gradients in the Southern Ocean. That study showed similar trends to ours: increased dynamic NPQ was associated with Fe-limited waters of the Antarctic Circumpolar Current, while subtropical gyre-type waters, where Fe was replete and nitrogen was low, exhibited subdued NPQ. Overall, they found that their NPQ parameterization showed the
545 strongest correlation with SST, which they interpreted to be largely caused by the relationship between SST and the extent of near-surface stratification and mixed layer depth (Browning et al., 2014). They also found a correlation between NPQ and Fv/Fm that was statistically significant at the p<0.001 confidence level, but was weaker than that with SST. It is worth pointing out that there were significant methodological differences between their approach and ours, as well as a much larger SST gradient in their study region (3-25°C), which likely has its own correlation with Fe limitation while also causing
550 differences in species composition that can have a strong influence on Fv/Fm (Suggett et al., 2009). Regardless of the cause in NPQ variability, our findings reinforce the observation by Browning et al. (2014) that NPQ can be highly variable due to factors other than incident PAR, implying that NPQ corrections that rely solely on PAR should be viewed with caution.

Overall, our results are consistent with the differences in NPQ observed in the two SST regimes being caused by differences
555 in their Fe limitation status, as evidenced in the respective Fv/Fm, with implications for the expected efficiency of

13

photochemistry. Not only did we find a strong inverse relationship between Fv/Fm and NPQ capacities estimated with an FRRf light-curve protocol, but the relationship was also borne out in NPQ_{SF} measured with a standard fluorometer – an instrument type frequently used on moorings, ships and autonomous measuring platforms such as Argo floats. We have thus shown that measurements from a standard fluorometer can provide useful information on phytoplankton physiology, in

560   particular the presence of Fe stress. While the phytoplankton community in our study was dominated by flagellates (Fig. 5), we expect that our results hold across a range of phytoplankton species, as the relationship between NPQ and Fe limitation status has been observed in laboratory and field studies elsewhere, including phytoplankton communities dominated by diatoms (Schuback et al., 2015, Schuback and Tortell, 2019).

565   **3.4. Case study: Application of NPQ_{SF} approach to mooring data**

In order to test further the utility of this interpretation of fluorescence measured with a standard fluorometer, we investigated NPQ_{SF} on a timeseries from the SOTS mooring (Fig. 9a). Here, NPQ_{SF} was estimated based on daily fluorescence measurements, after application of a smoothing filter (see Section 3.3.1). Due to differences in the maximum PAR on any given day, one could argue that NPQ_{SF} should be normalized by the incident PAR at F_{min}, as the depression in fluorescence is

570   expected to be proportional to the incident light. Such a measure decreases the scatter in the time series but preserves the overall trend observed in Fig. 9a) (Fig. S119). Note that noise in NPQ_{SF} is likely related to both fluctuating light conditions day to day and patchiness in phytoplankton fields. The fluorometer on the SOTS mooring measured once every hour, so only a very limited number of data points were available for any given day. The passages of small fronts and phytoplankton patches would thus have a large impact on the trends observed in a day, confounding the NPQ signal.

575

In the context of the ancillary measurements (Fig. 9), the trends observed in NPQ_{SF} over the growing season appear sensible. Some connection with changes in the MLD is apparent, for example a decrease in NPQ_{SF} in November as the mixed layer shoals, but the MLD dynamics cannot explain fluctuations in NPQ_{SF} over the summer. Nor does the light field experienced within the mixed layer (Fig. 9c) show a clear relationship with NPQ_{SF}. However, there is an interesting connection with the

580   dynamics in Chl-a concentrations: NPQ_{SF} is relatively low in spring and remains low, with some fluctuations, until Chl-a peaks in mid-January. After this peak, Chl-a decreases and NPQ_{SF} increases, a trend that could indicate the onset of Fe-limitation at the SOTS mooring late in summer. Indeed, several studies have concluded that the SAZ, in particular the SOTS area, is Fe-limited in summer (Boyd et al., 2001; Hutchins et al., 2001; Lannuzel et al., 2011; Sedwick et al., 1999), with Fe re-supply in winter from Ekman transport (Ellwood et al., 2008) and deep mixing (Tagliabue et al., 2014). An interpretation

585   of increased NPQ_{SF} as a response to the onset of Fe limitation is thus supported by the historical data available. Furthermore, we point out that the increase in NPQ_{SF} corresponds to an increase in water temperature over the season – the trend is thus opposite to the one seen in the voyage data, where NPQ_{SF} was highest in the colder waters. This further supports our contention that the observed trends in NPQ_{SF} (and Fv/Fm) are not driven by SST changes.

590   This same time period on the SOTS mooring has also been evaluated based on discrete samples for nutrients and phytoplankton, collected by an autonomous sampler (Eriksen et al., 2018). Of the macronutrients, only silicate decreased to concentrations that could be considered limiting (<1 μM at the end of January 2011). This development coincided with a decrease in diatom biovolume relative to other genera that lasted for about a month, but began to recover in March 2011 (Eriksen et al., 2018). Overall, the phytoplankton assemblage at SOTS in 2010/2011 was very diverse with diatoms,

595   dinoflagellates and ciliates figuring most prominently with respect to biovolume. Similarity-tests based on abundance indicated a spring community that was present until the end of 2010, followed by a summer community until the end of February, and a fall community thereafter (Eriksen et al., 2018). The observed fluctuations in NPQ_{SF} can thus not be tied to distinct changes in phytoplankton community.

14

600   To sum up, the findings from the SOTS mooring for the 2010/2011 season support our argument that NPQ_{SF} may hold information on phytoplankton physiology, as the observed fluctuations in NPQ_{SF} cannot be explained by developments in seasonal MLD, SST, light experienced in the mixed layer, or phytoplankton community composition. Rather, they exhibit a trend that is consistent with historical studies in the SAZ that have observed Fe limitation developing in summer and into autumn (see above), which could lead to an increased need for photoprotection, as evidenced in higher NPQ_{SF}.

605

4. Conclusions and future work

This study has explored the connection between NPQ and phytoplankton physiological status as indicated by Fv/Fm in an HNLC region. The results suggest that the variability observed in NPQ – mirroring changes in Fv/Fm – was driven by different levels of Fe limitation. A range of NPQ parameters was assessed, measured with both an active fluorometer (FRRf)
610 and a standard fluorometer mounted on the underway seawater supply of a research vessel. The relationship between NPQ and Fe limitation was tested with incubation experiments, where Fe concentrations were controlled by adding Fe and a strong Fe-binding ligand. All experiments showed a statistically significant relationship between Fe status and NPQ capacity as measured with an FRRf (Fig. 2), as has been observed previously (Schuback et al., 2015, Schuback and Tortell, 2019). Our analysis is novel in that it uses a standard fluorometer (such as is conventionally used to monitor Chl-a concentrations)
615 to derive the NPQ parameter NPQ_{SF}, linking its variability to phytoplankton physiology, i.e. Fe limitation status. Furthermore, application of the proposed methodology to data from a standard fluorometer on the SOTS mooring shows that the derived NPQ_{SF} exhibits a pattern that is consistent with the expected seasonal development of Fe limitation at the site. The approach may thus be promising for the interpretation of standard fluorometer data from HNLC regions, allowing assessment of the relative changes in Fe limitation status along voyage transects and mooring timeseries. Interpretation of
620 fluorescence data in this way will be improved by independent assessments of Chl-a concentration, such as can be achieved with an ac-9. Normalization by Chl-a (or phytoplankton absorption) removes the influence of Chl-a concentration on the fluorescence signal, thus refining the NPQ signal. Overall, our results point to a novel approach for the interpretation of widely available fluorescence sensor data to assess the role of Fe sufficiency in phytoplankton physiology, and thus productivity, in the Southern Ocean.

625

Ultimately, this approach to fluorescence has the potential to be applied to data from autonomous floats in the Southern Ocean, such as the BGC-Argo fleet. A recent application to glider data from the SAZ in the Atlantic Ocean has allowed identification of regions and time periods where Fe limitation was relieved (Ryan-Keogh and Thomalla, in prep). Studies of this kind will improve our understanding of biogeochemical cycles in the understudied Southern Ocean. However, care will
630 undoubtedly be needed in the interpretation of large spatial variations (e.g., when crossing fronts) owing to differences in species composition and mixing regimes.

Future work should include laboratory experiments under fluctuating light conditions, i.e. mimicking mixing in the ocean, to further probe the interplay of light history and Fe status on NPQ and how both affect phytoplankton growth. Care should be
635 taken to not only focus on steady state scenarios, but to also include perturbation experiments, as relaxation of Fe limitation in the Southern Ocean may be a sporadic event, for example if storm-induced deep mixing or dust deposition are the means of Fe fertilization. Overall, assessment of the level of Fe limitation is less interesting than the question how this limitation affects primary production and growth rate, as these are the quantities that will be felt throughout the ecosystem. The eventual goal would thus be to establish a link between a readily measurable proxy, such as NPQ_{SF}, and phytoplankton
640 growth. This could be achieved by further investigations into the relationship between NPQ and the maximum quantum yield of photosynthesis, which has been shown to respond to Fe fertilization (Alderkamp et al., 2009; Hiscock et al., 2008)

15

and has also been incorporated into a new global model of net primary production, albeit currently as a function of light acclimation only (Silsbe et al., 2016).

Data availability

645 All voyage data (except FRRf and ac-9) are freely available from the CSIRO Data Trawler: https://www.cmar.csiro.au/data/trawler/survey_details.cfm?survey=IN2018_V02. The mooring data are freely available via the Australian Ocean Data Network portal: https://portal.aodn.org.au. FRRf and ac-9 data are available directly from the corresponding author and can be requested by email: christina.schallenberg@utas.edu.au.

650

Author contributions

CS conceived the idea for the study and designed and carried out the experimental work on the voyage except for ^{14}C uptake experiments, which were done by RFS. CS processed and analysed all data post voyage with the following exceptions: phytoplankton pigment and filter pad absorption measurements were undertaken and interpreted by LAC, and the results of 655 ^{14}C uptake experiments were analysed by RFS. TT leads the Southern Ocean Times Series facility which provided the moored sensor observations. The details of the inquiry were significantly improved through discussions with RFS, NS, TWT and PWB. CS wrote the majority of the manuscript, with refinements and additions provided by all co-authors.

Competing interests

The authors declare that they have no conflict of interest.

References

680 Alderkamp, A.-C., Kulk, G., Buma, A. G. J., Visser, R. J. W., Van Dijken, G. L., Mills, M. M., and Arrigo, K. R.: The effect of iron limitation on the photophysiology of *Phaeocystis antarctica* (Prymnesiophyceae) and *Fragilariopsis cylindrus* (Bacillariophyceae) under dynamic irradiance, J. Phycol., 48(1), 45–59, https://doi.org/10.1111/j.1529-8817.2011.01098.x, 2012.
Alderkamp, A.-C., Van Dijken, G. L., Lowry, K. E., Lewis, K. M., Joy-Warren, H. L., van de Poll, W., … Arrigo, K. R.: 685 Effects of iron and light availability on phytoplankton photosynthetic properties in the Ross Sea. Mar. Ecol. Prog. Ser., 621, 33–50, 2019.
Barlow, R., Kyewalyanga, M., Sessions, H., van den Berg, M., and Morris, T.: Phytoplankton pigments, functional types,

and absorption properties in the Delagoa and Natal Bights of the Agulhas ecosystem. Estuar. Coast. Shelf. S., 80(2), 201–211. https://doi.org/10.1016/j.ecss.2008.07.022, 2008.

690   Behrenfeld, M. J., and Kolber, Z. S.: Widespread iron limitation of phytoplankton in the South Pacific Ocean. Science, 283, 840–844, 1999.

Behrenfeld, M. J. M., and Milligan, A. A. J.: Photophysiological expressions of iron stress in phytoplankton. Ann. Rev. Mar. Sci., 5, 217–246, https://doi.org/10.1146/annurev-marine-121211-172356, 2013.

Behrenfeld, M. J., Westberry, T. K., Boss, E. S., O'Malley, R. T., Siegel, D. A., Wiggert, J. D., … Mahowald, N.: Satellite-
695   detected fluorescence reveals global physiology of ocean phytoplankton. Biogeosciences, 6(5), 779–794, https://doi.org/10.5194/bg-6-779-2009, 2009.

Biermann, L., Guinet, C., Bester, M., Brierley, A., and Boehme, L.: An alternative method for correcting fluorescence quenching. Ocean Sci., 11, 83–91, https://doi.org/10.5194/os-11-83-2015, 2015.

Boyd, P. W., and Harrison, P. J.: Phytoplankton dynamics in the NE subarctic Pacific. Deep-Sea Res. Pt. II, 46, 2405–2432,
700   1999.

Bowie, A. R., Lannuzel, D., Remenyi, T. A., Wagener, T., Lam, P. J., Boyd, P. W., … Trull, T. W.: Biogeochemical iron budgets of the Southern Ocean south of Australia: Decoupling of iron and nutrient cycles in the subantarctic zone by the summertime supply. Global Biogeochem. Cy., 23, https://doi.org/10.1029/2009GB003500, 2009.

Boyd, P. W., and Abraham, E. R.: Iron-mediated changes in phytoplankton photosynthetic competence during SOIREE.
705   Deep-Sea Res. Pt. II, 48(11–12), 2529–2550, https://doi.org/10.1016/S0967-0645(01)00007-8, 2001.

Boyd, P. W., Crossley, A. C., DiTullio, G. R., Griffiths, F. B., Hutchins, D. A., Queguiner, B., … Trull, T. W.: Control of phytoplankton growth by iron supply and irradiance in the subantarctic Southern Ocean: Experimental results from the SAZ project. J. Geophys. Res.-Oceans, 106(C12), 31573–31583, 2001.

Boyd, P. W., Jickells, T., Law, C. S., Blain, S., Boyle, E. A, Buesseler, K. O., … Watson, A. J.: Mesoscale iron enrichment
710   experiments 1993-2005: Synthesis and future directions. Science, 315(5812), 612–617, https://doi.org/10.1126/science.1131669, 2007.

Boyd, P. W., Rynearson, T. A., Armstrong, E. A, Fu, F., Hayashi, K., Hu, Z., … Thomas, M. K.: Marine phytoplankton temperature versus growth responses from polar to tropical waters--outcome of a scientific community-wide study. PLOS ONE, 8(5), e63091, https://doi.org/10.1371/journal.pone.0063091, 2013.

715   Browning, T., Bouman, H., and Moore, C.: Satellite-detected fluorescence: decoupling nonphotochemical quenching from iron stress signals in the South Atlantic and Southern Ocean. Global Biogeochem. Cy., 28, 510–524. https://doi.org/10.1002/2013GB004773.Received, 2014.

Clementson, L. A. (2013). The CSIRO method, in The Fifth SeaWiFS HPLC Analysis Round-Robin Experiment (SeaHARRE-5); NASA Technical Memorandum 2012-217503, edited by: Hooker, S. B. et al., NASA Goddard Space
720   Flight Center, Greenbelt, Maryland.

Davison, I.R.: Environmental effects on algal photosynthesis: temperature. J. Phycol., 27, 2–8, (1991).

Demmig-Adams, B., Garab, G., Adams III, W., and Govindjee (Eds.): Non-Photochemical Quenching and Energy Dissipation in Plants, Algae and Cyanobacteria, Springer, https://doi.org/10.1007/978-94-017-9032-1, 2014.

Ellwood, M. J., Boyd, P. W., and Sutton, P.: Winter-time dissolved iron and nutrient distributions in the Subantarctic Zone
725   from 40 – 52S ; 155 – 160E. Geophys. Res. Lett., 35(L11604), 1–6, https://doi.org/10.1029/2008GL033699, 2008.

Ellwood, M. J., Strzepek, R. F., Strutton, P. G., Trull, T. W., Fourquez, M., and Boyd, P. W.: Biogeochemical metrics reveal distinctive but unusual iron cycling in Southern Ocean eddies. *Submitted to Nat. Commun*.

Eriksen, R., Trull, T. W., Davies, D., Jansen, P., Davidson, A. T., Westwood, K., and van den Enden, R.: Seasonal succession of phytoplankton community structure from autonomous sampling at the Australian Southern Ocean Time
730   Series (SOTS) observatory. Mar. Ecol. Prog. Ser., 589, 13–31, 2018.

Falkowski, P., Lin, H., and Gorbunov, M.: What limits photosynthetic energy conversion efficiency in nature? Lessons from the oceans. Philos. T. Roy. Soc. B, 372, 2-8, 2017.

Geider, R. J., La Roche, J., Greene, R. M., and Olaizola, M.: Response of the photosynthetic apparatus of *Phaeodactylum tricornutum* (Bacillariophyceae) to nitrate, phosphate, or iron starvation. J. Phycol., 29, 755-766, 1993.

735   Greene, R. M., Geider, R. J., Kolber, Z., and Falkowski, P. G.: Iron-Induced changes in light harvesting and photochemical energy-conversion processes in eukaryotic marine algae. Plant Physiol., 100, 565-575, 1992.

Grenier, M., Della Penna, A., and Trull, T. W.: Autonomous profiling float observations of the high-biomass plume downstream of the Kerguelen Plateau in the Southern Ocean. Biogeosciences, 12, 2707–2735, https://doi.org/10.5194/bg-12-2707-2015, 2015.

740   Hassler, C. S., Ridgway, K. R., Bowie, A. R., Butler, E. C. V., Clementson, L. A., Doblin, M. A., Davies, D. M., Law, C., Ralph, P., J., van der Merwe, P., Watson, R., and Ellwood, M. J.: Primary productivity induced by iron and nitrogen in the Tasman Sea: an overview of the PINTS expedition. Mar. Freshwater Res., 65, 517-537, 2014.

Herraiz-Borreguero, L., and Rintoul, S. R.: Regional circulation and its impact on upper ocean variability south of Tasmania. Deep-Sea Res. Pt. II, 58(21–22), 2071–2081, https://doi.org/10.1016/j.dsr2.2011.05.022, 2011.

745   Hiscock, M. R., Lance, V. P., Apprill, A. M., Bidigare, R. R., Johnson, Z. I., Mitchell, B. G., … Barber, R. T.: Photosynthetic maximum quantum yield increases are an essential component of the Southern Ocean phytoplankton response to iron. P. Natl. Acad. Sci. USA, 105(12), 4775–4780, 2008.

Holm-Hansen, O., Lorenzen, C.J., Holmes, R.W., and Strickland, J.D.H.: Fluorometric determination of Chlorophyll, ICES J. Mar. Sci., 30, 3-15, 1965.

750   Horton, P., Ruban, A. V., and Walters, R. G.: Regulation of light harvesting in green plants. Annu. Rev. Plant Physio., 47(1), 655–684, https://doi.org/10.1146/annurev.arplant.47.1.655, 1996.

Huot, Y., Franz, B. A., and Fradette, M.: Estimating variability in the quantum yield of Sun-induced chlorophyll fluorescence: A global analysis of oceanic waters. Remote Sens. Environ., 132, 238–253, https://doi.org/10.1016/j.rse.2013.01.003, 2013.

755 Hutchins, D. A., Sedwick, P. N., DiTullio, G. R., Boyd, P. W., Queguiner, B., Griffiths, F. B., and Crossley, C.: Control of phytoplankton growth by iron and silicic acid availability in the subantarctic Southern Ocean: Experimental results from the SAZ project. J. Geophys. Res.-Oceans, 106(C12), 31559–31572, 2001.

Jeffrey, S., and Humphrey, G.: New spectrophotometric equations for determining chlorophyll a, b, c1 and c2 in higher plants, algae and natural phytoplankton. Biochem. Physiol. Pflanzen, 167, 191–194, 1975.

760 Kishino, M., Takahashi, M., Okami, M., and Ischimura, S.: Estimation of the spectral absorption coefficients of phytoplanktonin the sea. B. Mar. Sci., 37, 634–642, 1985.

Kolber, Z. S., Barber, R. T., Coale, K. H., Fitzwater, S. E., Greene, R. M., Johnson, K. S., … Falkowski, P. G.: Iron limitation of phytoplankton photosynthesis in the equatorial Pacific Ocean. Nature, 371, 145–149, 1994.

Krause, G. H., and Weis, E.: Chlorophyll fluorescence as a tool in plant physiology - II. Interpretation of fluorescence
765 signals. Photosynth. Res., 5(2), 139–157, https://doi.org/10.1007/BF00028527, 1984.

Kropuenske, L. R., Mills, M. M., Van Dijken, G. L., Bailey, S., Robinson, D. H., Welschmeyer, N. A., and Arrigo, K. R.: Photophysiology in two major Southern Ocean phytoplankton taxa: Photoprotection in *Phaeocystis antarctica* and *Fragilariopsis* cylindrus. Limnol. Oceanogr., 54(4), 1176–1196, 2009.

Kulk, G., De Vries, P., Van De Poll, W. H., Visser, R. J. W., and Buma, A. G. J.: Temperature-dependent growth and
770 photophysiology of prokaryotic and eukaryotic oceanic picophytoplankton. Mar. Ecol. Progr. Ser., 466, 43–55, https://doi.org/10.3354/meps09898, 2012.

Lannuzel, D., Bowie, A. R., Remenyi, T., Lam, P., Townsend, A., Ibisanmi, E., … Schoemann, V.: Distributions of dissolved and particulate iron in the sub-Antarctic and Polar Frontal Southern Ocean (Australian sector). Deep-Sea Res. Pt. II, 58, 2094–2112, https://doi.org/10.1016/j.dsr2.2011.05.027, 2011.

775 Laws, E. A.: Photosynthetic quotients, new production and net community production in the open ocean, Deep-Sea Res., 38, 143–167, 1991.

Letelier, R. M., Abbott, M., and Karl, D. M.: Chlorophyll natural fluorescence response to upwelling events in the Southern Ocean. Geophys. Res. Lett. 24(4), 409–412, 1997.

Martínez-García, A., Sigman, D. M., Ren, H., Anderson, R. F., Straub, M., Hodell, D. A., … Haug, G. H.: Iron fertilization
780 of the subantarctic ocean during the last Ice Age. Science, 343, 1347–1350, 2014.

Mendes, C. R. B., Kerr, R., Tavano, V. M., Carvalheiro, F. A., Garcia, C. A. E., Dessai, D. R. G., and Anilkumar, N.: Cross-front phytoplankton pigments and chemotaxonomic groups in the Indian sector of the Southern Ocean. Deep-Sea Res. Pt. II, 118, 221–232, https://doi.org/10.1016/j.dsr2.2015.01.003, 2015.

Milligan, A., Aparicio, U., and Behrenfeld, M.: Fluorescence and nonphotochemical quenching responses to simulated
785 vertical mixing in the marine diatom Thalassiosira weissflogii. Mar. Ecol. Progr. Ser., 448, 67–78. https://doi.org/10.3354/meps09544, 2012.

Mitchell, B.: Algorithms for determining the absorption coefficient for aquatic particulates using the quantitative filter technique. Proc. SPIE, 1302, 137–148, 1990.

Moore, C. M., Mills, M. M., Arrigo, K. R., Berman-Frank, I., Bopp, L., Boyd, P. W., … Ulloa, O.: Processes and patterns of
790 oceanic nutrient limitation. Nat. Geosci., 6, 1–10, https://doi.org/10.1038/ngeo1765, 2013.

Morel, A., Huot, Y., Gentili, B., Werdell, P.J., Hooker, S.B., and Franz, A.B: Examining the consistency of products derived from various ocean color sensors in open ocean (Case 1) waters in the perspective of a multi-sensor approach, Remote Sens. Environ., 111, 69-88, 2007.

Morrison, J. R.: In situ determination of the quantum yield of phytoplankton chlorophyll a fluorescence: A simple algorithm,
795 observations, and a model. Limnol. Oceanogr., 48(2), 618–631. https://doi.org/10.4319/lo.2003.48.2.0618, 2003.

Morrison, J. R., and Goddwin, D. S.: Phytoplankton photocompensation from space-based fluorescence measurements. Geophys. Res. Lett., 37, L06603, 2010.

Müller, P., Li, X., and Niyogi, K.: Non-photochemical quenching. A response to excess light energy. Plant Physiol., 125, 1558-1566, 2001.

800 O'Malley, R. T., Behrenfeld, M. J., Westberry, T. K., Milligan, A. J., Shang, S., and Yan, J.: Geostationary satellite observations of dynamic phytoplankton photophysiology. Geophys. Res. Lett., 41(14), 5052–5059, https://doi.org/10.1002/2014GL060246, 2014.

Oxborough, K., and Baker, N. R.: Resolving chlorophyll a fluorescence images of photosynthetic efficiency into photochemical and non-photochemical components – calculation of qP and Fv' / Fm' without measuring Fo'.
805 Photosynth. Res., 54, 135–142, 1997.

Petrou, K., Trimborn, S., Rost, B., Ralph, P. J., and Hassler, C. S.: The impact of iron limitation on the physiology of the Antarctic diatom *Chaetoceros simplex*. Mar. Biol., 161(4), 925–937, https://doi.org/10.1007/s00227-014-2392-z, 2014.

Raven, J. A., and Geider, R. J.: Temperature and algal growth. New Phytol., 110, 441–461, 1988.

Rees, C., Pender, L., Sherrin, K., Schwanger, C., Hughes, P., Tibben, S., … Rayner, M.: Methods for reproducible shipboard
810 SFA nutrient measurement using RMNS and automated data processing. Limnol. Oceanogr.-Meth, 17(1), 25–41, https://doi.org/10.1002/lom3.10294, 2019.

Roesler, C. S., and Barnard, A. H.: Optical proxy for phytoplankton biomass in the absence of photophysiology: Rethinking the absorption line height. Methods in Oceanography, 7, 79–94, https://doi.org/10.1016/j.mio.2013.12.003, 2013.

Roesler, C., Uitz, J., Claustre, H., Boss, E., Xing, X., Organelli, E., … Barbieux, M.: Recommendations for obtaining
815 unbiased chlorophyll estimates from in situ chlorophyll fluorometers: A global analysis of WET Labs ECO sensors.

Limnol. Oceanogr.-Meth., 15(6), 572–585, https://doi.org/10.1002/lom3.10185, 2017.

Rohacek, K.: Chlorophyll fluorescence parameters: The definitions, photosynthetic meaning, and mutual relationships. Photosynthetica, 40(1), 13–29, 2002.

820 Rose, J. M., Feng, Y., DiTullio, G. R., Dunbar, R. B., Hare, C. E., Lee, P. A., … Hutchins, D. A.: Synergistic effects of iron and temperature on Antarctic phytoplankton and microzooplankton assemblages. Biogeosciences, 6, 3131–3147. https://doi.org/10.5194/bg-6-3131-2009, 2009.

Ryan-Keogh, T. J., DeLizo, L. M., Smith Jr., W. O., Sedwick, P. N., McGillicuddy Jr., D. J., Moore, C. M., and Bibby, T. S.: Temporal progression of photosynthetic-strategy in phytoplankton in the Ross Sea, Antarctica. J. Mar. Sys., 166, 87–96, https://doi.org/10.1016/j.jmarsys.2016.08.014, 2017.

825 Ryan-Keogh, T. J., and Thomalla, S. J.: Deriving a proxy for iron limitation from passive chlorophyll fluorescence on buoyancy gliders, in prep.

Schallenberg, C., Jansen, P., and Trull, T. W.: Southern Ocean Time Series (SOTS) Quality Assessment and Control Report Wetlabs FLNTUS instruments Version 2.0. https://doi.org/10.26198/5c4a932ca8ae4, 2019.

Schallenberg, C., Lewis, M. R., Kelley, D. E., and Cullen, J. J.: Inferred influence of nutrient availability on the relationship 830 between Sun-induced chlorophyll fluorescence and incident irradiance in the Bering Sea. J. Geophys. Res.-Oceans, 113(C7), C07046, https://doi.org/10.1029/2007JC004355, 2008.

Schuback, N., Schallenberg, C., Duckham, C., Maldonado, M. T., and Tortell, P. D.: Interacting effects of light and iron availability on the coupling of photosynthetic electron transport and CO_2-assimilation in marine phytoplankton. PLOS ONE, 10, e0133235, https://doi.org/10.1371/journal.pone.0133235, 2015.

835 Schuback, N., and Tortell, P. D.: Diurnal regulation of photosynthetic light absorption, electron transport and carbon fixation in two contrasting oceanic environments. Biogeosciences, 16, 1381–1399, https://doi.org/10.5194/bg-2018-524, 2019.

Sedwick, P., DiTullio, G., Hutchins, D., Boyd, P., Griffiths, F., Crossley, A. C., … Queguiner, B.: Limitation of algal growth by iron deficiency in the Australian Subantarctic region. Geophys. Res. Lett., 26(18), 2865–2868, 1999.

Shadwick, E. H., Trull, T. W., Tilbrook, B., Sutton, A. J., Schulz, E., and Sabine, C. L.: Seasonality of biological and 840 physical controls on surface ocean CO_2 from hourly observations at the Southern Ocean Time Series site south of Australia. Global Biogeochem. Cy., 29(2), 223–238, https://doi.org/10.1002/2014GB004906, 2015.

Sigman, D. M., and Boyle, E. A.: Glacial/interglacial variations in atmospheric carbon dioxide. Nature, 407, 859–869, 2000.

Silsbe, G., Behrenfeld, M., Halsey, K., Milligan, A., and Westberry, T. K.: The CAFE model: A net production model for global ocean phytoplankton. Global Biogeochem. Cy., 30, 1756–1777, https://doi.org/10.1002/2016GB005521, 2016.

845 Slade, W., Boss, E., Dall'Olmo, G., Langner, M., Loftin, J., Behrenfeld, M., … Westberry, T.: Underway and moored methods for improving accuracy in measurement of spectral particulate absorption and attenuation. J. Atmos. Ocean. Tech., 27, 1733–1746, https://doi.org/10.1175/2010JTECHO755.1, 2010.

Strzepek, R. F., Boyd, P. W., and Sunda, W. G.: Photosynthetic adaptation to low iron, light, and temperature in Southern Ocean phytoplankton. P. Natl. Acad. Sci. USA, 116(10), 4388-4393, 2019.

850 Strzepek, R. F., Hunter, K. A., Frew, R. D., Harrison, P. J., and Boyd, P. W.: Iron-light interactions differ in Southern Ocean phytoplankton. Limnol. Oceanogr., 57(4), 1182–1200, https://doi.org/10.4319/lo.2012.57.4.1182, 2012.

Suggett, D. J., Moore, C. M., Hickman, A. E., and Geider, R. J.: Interpretation of fast repetition rate (FRR) fluorescence: signatures of phytoplankton community structure versus physiological state. Mar. Ecol. Progr. Ser., 376, 1–19, https://doi.org/10.3354/meps07830, 2009.

855 Tagliabue, A., Sallée, J., Bowie, A., and Lévy, M.: Surface-water iron supplies in the Southern Ocean sustained by deep winter mixing. Nat. Geosci., 7, 314–320, https://doi.org/10.1038/NGEO2101, 2014.

Thomalla, S. J., Moutier, W., Ryan-Keogh, T. J., Gregor, L., and Schütt, J.: An optimized method for correcting fluorescence quenching using optical backscattering on autonomous platforms. Limnol. Oceanogr.-Meth., 16, 132–144, https://doi.org/10.1002/lom3.10234, 2018.

860 Trees, C. C., Kennicutt, M. C., and Brooks, J. M.: Errors associated with the standard fluorimetric determination of chlorophylls and phaeopigments. Mar. Chem., 17(1), 1–12, https://doi.org/10.1016/0304-4203(85)90032-5, 1985.

Weeding, B., and Trull, T. W.: Hourly oxygen and total gas tension measurements at the Southern Ocean Time Series site reveal winter ventilation and spring net community production. J. Geophys. Res.-Oceans, 119(1), 348–358, https://doi.org/10.1002/2013JC009302, 2014.

865 Westwood, K. J., Griffiths, F. B., Webb, J. P., and Wright, S. W.: Primary production in the Sub-Antarctic and Polar Frontal Zones south of Tasmania, Australia; SAZ-Sense survey, 2007. Deep-Sea Res. Pt. II, 58, 2162–2178, 20072011.

Xing, X., Briggs, N., Boss, E., and Claustre, H.: Improved correction for non-photochemical quenching of in situ chlorophyll fluorescence based on a synchronous irradiance profile. Opt. Express, 26(19), 24734, https://doi.org/10.1364/oe.26.024734, 2018.

870 Xing, X., Claustre, H., Blain, S., D'Ortenzio, F., Antoine, D., Ras, J., and Guinet, C. : Quenching correction for in vivo chlorophyll fluorescence acquired by autonomous platforms: A case study with instrumented elephant seals in the Kerguelen region (Southern Ocean). Limnol. Oceanogr.-Meth., 10, 483–495, https://doi.org/10.4319/lom.2012.10.483, 2012.

875

Table 1. Details of incubation experiments

Experiment no.	Date (UTC)	Sampling Time (UTC)	Sampled how	SST (°C)	Light level (% of surface)	Duration (h)	Starting Chl-a concentration (mg m^{-3})	Initial Fv/Fm
1	6-3-2018	20:30	TMR (35 m)	10.7	67	53	0.35	0.33
2	8-3-2018	18:40	FISH	11.2	67	55	0.30	0.32
3	13-3-2018	22:30	FISH	10.5	25	51.5	0.37	0.34

880

20

Table 2. List of fluorescence-related parameters derived and discussed

	Parameter	Units	Method
σ_{PSII}	Functional absorption cross section of PSII	$nm^2\ RC^{-1}$	FRRf ST protocol during dark-regulated state
F	Fluorescence	Arbitrary	Measured with a standard fluorometer with minimal or no dark-acclimation period
F_{min}	Minimum fluorescence in the day (at high light)	Arbitrary	Measured with a standard fluorometer, with minimal or no dark-acclimation
F_{max}	Maximum fluorescence in the day (at low light)	Arbitrary	Measured with an standard fluorometer, with minimal or no dark-acclimation
Fv/Fm	Maximum quantum yield of PSII	No units	FRRf ST protocol during dark-regulated state; $(F_m - F_o)/F_m$
NPQ	Non-photochemical quenching	No units	Term comprising a number of non-photochemical quenching processes that decrease fluorescence at supersaturating light intensities (e.g. Fm' relative to Fm, and Fmin relative to Fmax)
$NPQ_{NSV}(750)$, $NPQ_{NSV}(1000)$	Normalized Stern-Volmer NPQ at light intensities of 750 and 1000 μmol quanta $m^{-2}\ s^{-1}$	No units	FRRf ST protocol during light-regulated state; Eq (3)
$NPQ_{SV}(750)$, $NPQ_{SV}(1000)$	Stern-Volmer NPQ at light intensities of 750 and 1000 μmol quanta $m^{-2}\ s^{-1}$	No units	FRRf ST protocol during light-regulated state; Eq (2)
NPQ_{SF}	NPQ analogous to Stern-Volmer NPQ	No units	Measured with a standard fluorometer with minimal or no dark-acclimation; calculated as $(F_{max} - F_{min})/F_{min}$
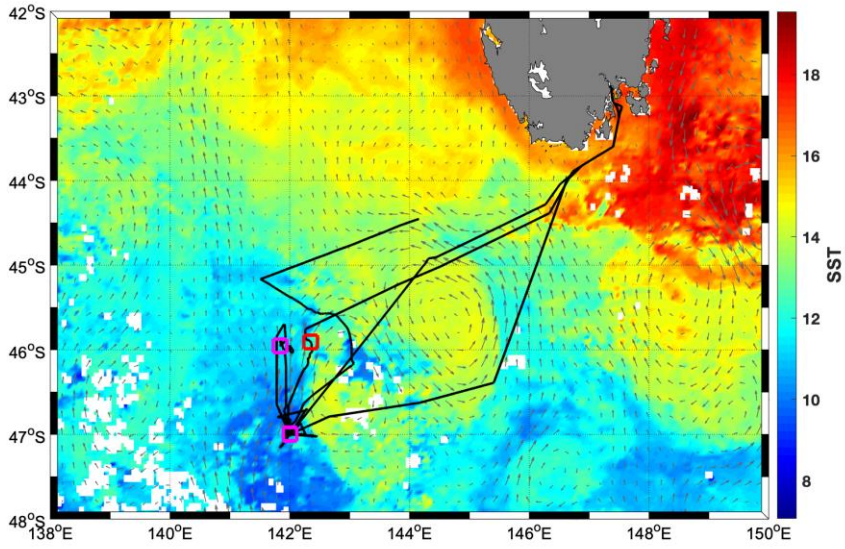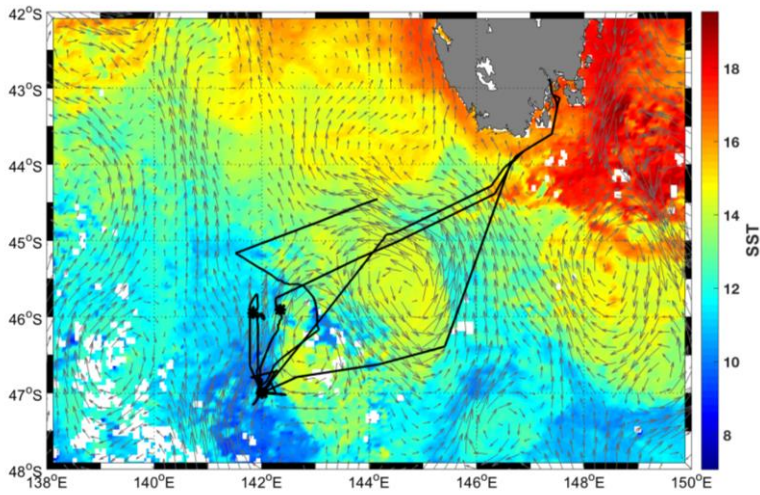
Figure 1: Average Sea Surface Temperature (SST) for March 2018 from the MODIS-Aqua satellite, overlain with geostrophic currents for March 16, 2018 (grey arrows) and the cruise track (black line) as well as CTD locations in the cold water mass (purple squares) and in the warm water mass (red square)(black asterisks). Surface geostrophic velocities (IMOS-OceanCurrent-

22

890   **Gridded sea level anomaly-Delayed mode) were downloaded from the AODN data portal at https://portal.aodn.org.au. Credit: IMOS and CSIRO. References: http://oceancurrent.imos.org.au/**
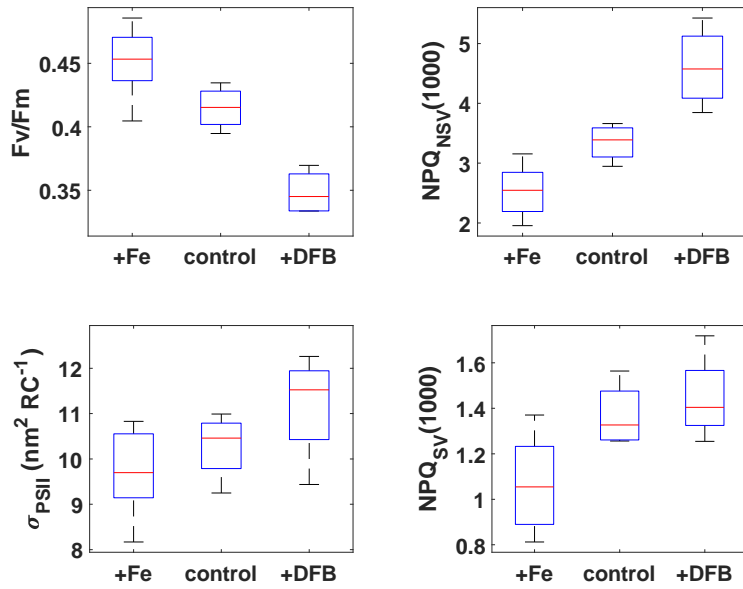
895

Figure 2: FRRf results after ~53 hours for the 3 pooled incubation experiments. The respective treatments are indicated on the x-axes (2 nM and 0.2 nM Fe additions were pooled into +Fe), and measured parameters are on the y-axes. NPQ capacity was ~~measured~~ estimated at 1000 µmol quanta m^{-2} s^{-1} after 24-minute exposure to increasing actinic light intensities (see Fig. S2 for details of the fluorescence light curves). Boxplots show the sample medians in red, with the blue boxes indicating the 25th and 75th

900 **percentiles; whiskers extend to the most extreme data points. All +Fe treatments were significantly different from the respective DFB treatments (Wilcoxon rank sum test, p<0.05), and except for σ_{PSII}, all +Fe treatments were also significantly different from the respective control treatments.**

905
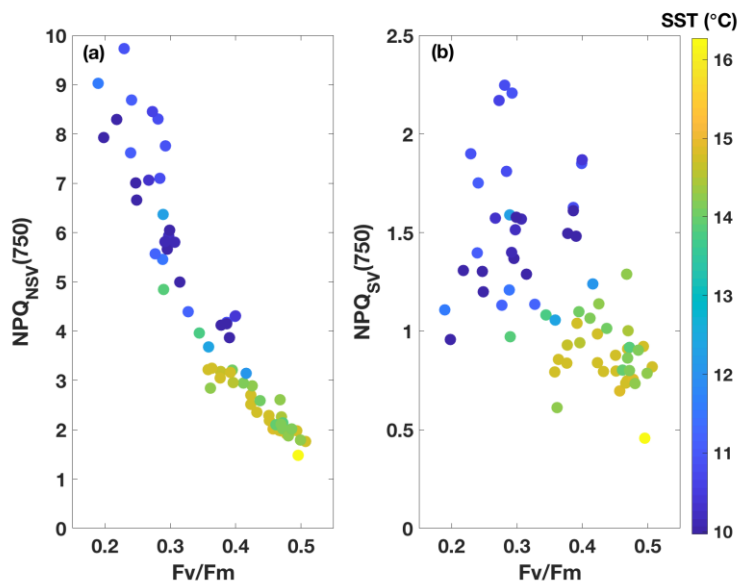
Figure 3: FRRf results from underway samples (n=66). NPQ capacity at a light intensity of 750 μmol quanta m^{-2} s^{-1} is plotted against Fv/Fm, with two different NPQ parameterizations used: Normalized Stern-Volmer (a) and Stern-Volmer (b). Colour indicates SST of the corresponding waters.

910
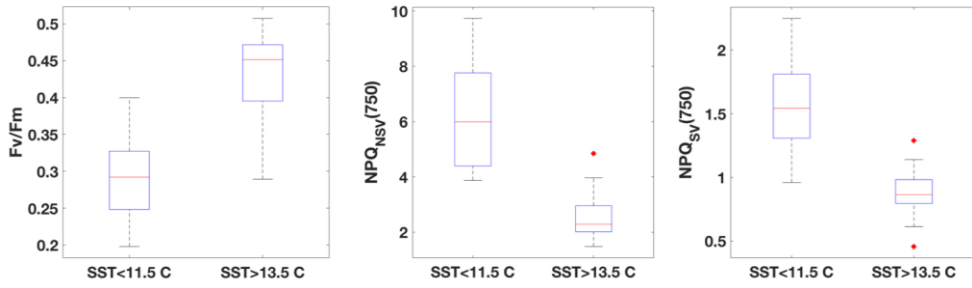
915   **Figure 4: Comparison of FRRf data from underway samples, grouped based on SST. All parameters are significantly different between the two respective water masses (Wilcoxon rank sum test, p<<0.01).**
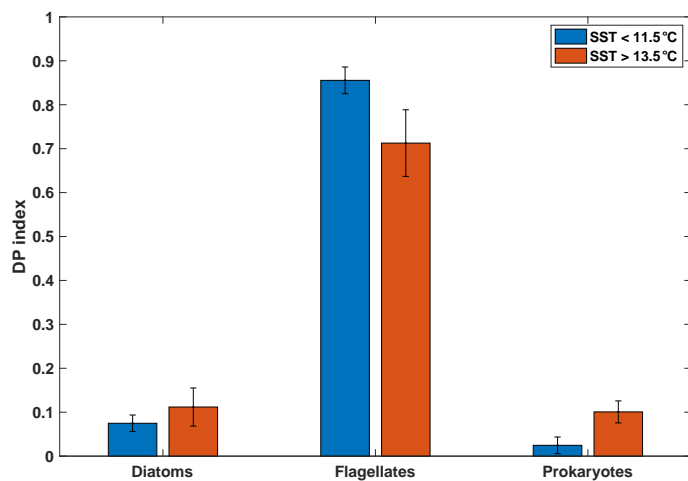
920

Figure 5: Mean diagnostic pigment (DP) indices calculated based on pigment ratios from HPLC analyses for samples taken from the underway seawater supply, grouped by SST (n=6 for SST>13.5°C, n=7 for SST<11.5°C). Error bars indicate one standard deviation. See section 2.4.2 for calculation of the DP index.

925

930
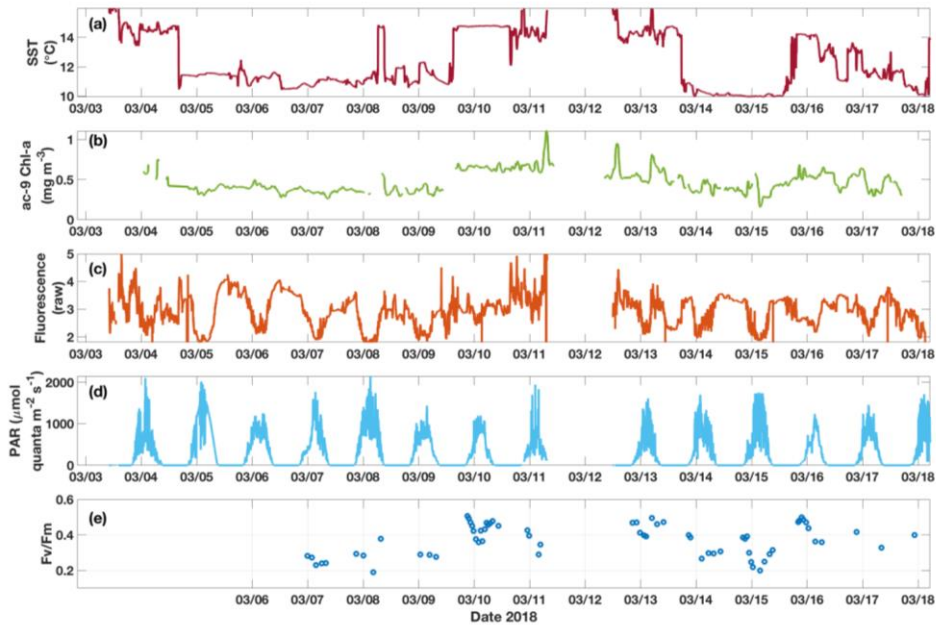
Figure 6: Time series for underway data from the SOTS cruise in 2018 of a) SST, b) Chl-a from ac-9, c) raw fluorescence, d) above-water PAR, and e) Fv/Fm measured on dark-~~adapted~~ acclimated discrete samples. Diel fluctuations in fluorescence are apparent, especially when cold water was sampled. These fluctuations are not found in the corresponding Chl-a time series. Note
935 **that the data gap around March 12 is due to the ship leaving the SAZ region during that time.**

28
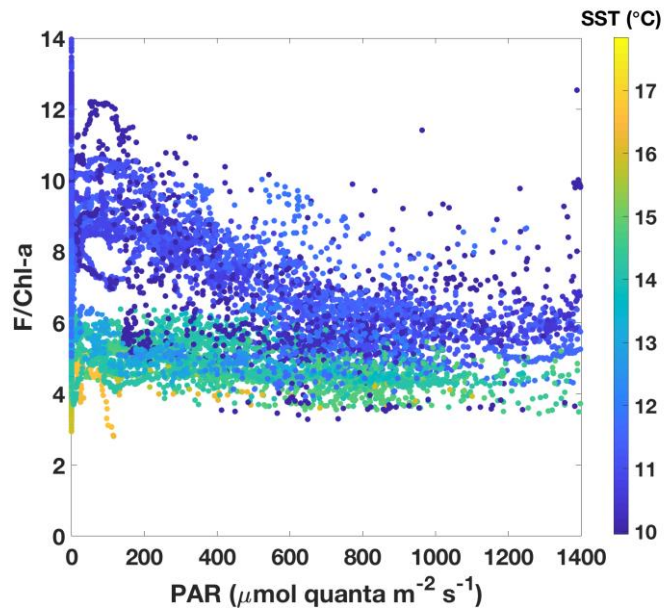
940 **Figure 7: Underway fluorescence data normalized to Chl-a plotted against incident PAR above the surface. Chl-a was estimated from ac-9 data. Data points are colour-coded according to SST.**
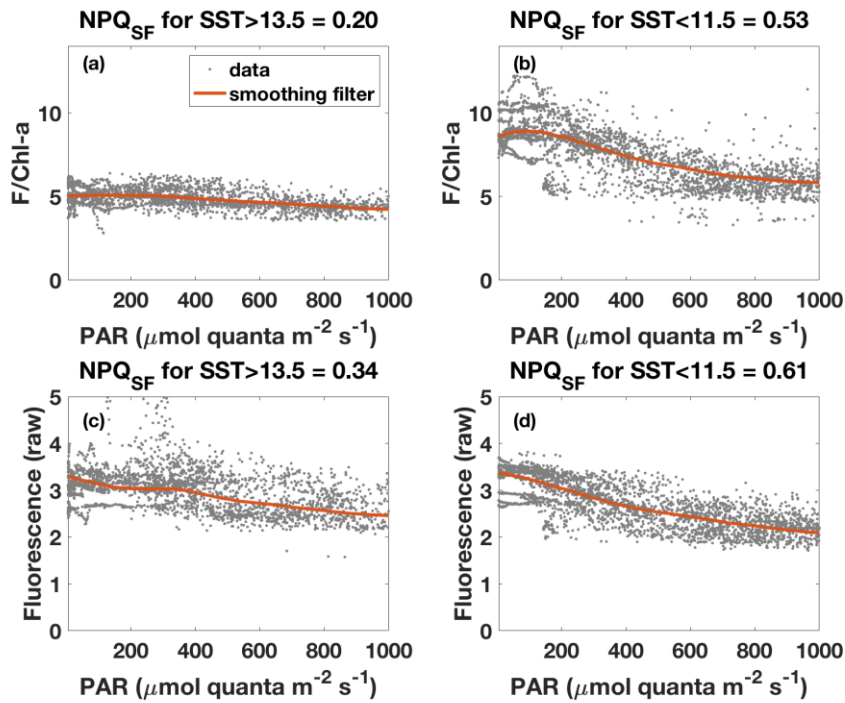
Figure 8: Fluorescence-PAR relationship as in Figure 7, but with data grouped according to the respective SST (grey dots), and with a robust Loess smoothing filter applied to the ordered data (red). Note that data for PAR <5 μmol quanta m^{-2} s^{-1} are not shown. Panels a) and b) show the results for fluorescence normalized to Chl-a (estimated based on ac-9 data), while panels c) and d) show results for unnormalized fluorescence. NPQ$_{SF}$ was calculated according to Eqn (6) using the smoothed data, with F$_{max}$ the maximum fluorescence for PAR>5 and PAR <1000 μmol quanta m^{-2} s^{-1} while F$_{min}$ was taken as the minimum fluorescence for that range.
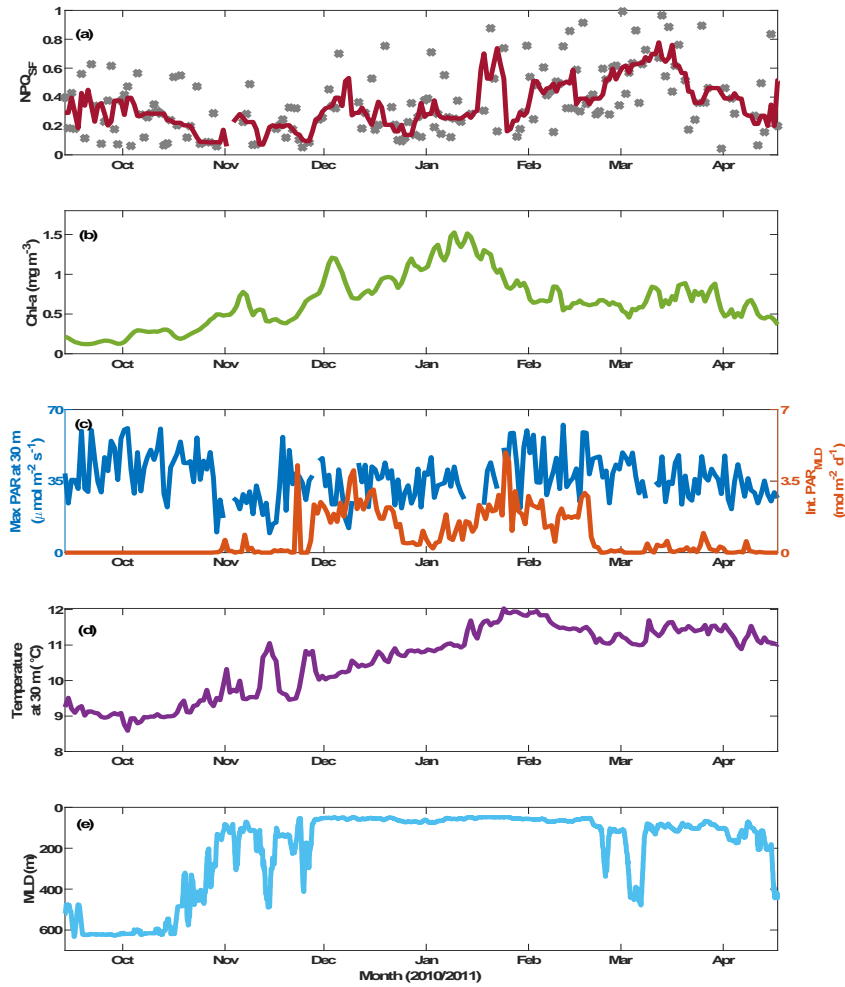
Figure 9: SOTS mooring data for October 2010 to April 2011. Panel a) shows NPQ$_{SF}$ (see Figure S119 for a version where NPQ$_{SF}$ is normalized to PAR at F$_{min}$), with grey markers indicating daily estimates and the red line a 7-day running median. Panel b) shows a 3-point running mean over daily Chl-a concentrations estimated based on calibrated fluorescence; panel c) shows maximum PAR recorded at 30 m for any given day (left axis) and the integrated daily PAR for the mixed layer (right axis), with incident PAR calculated based on latitude, longitude, time of year and clear sky conditions, PAR attenuation estimated as a function of Chl-a based on Morel et al. (2007), and MLD as in panel e). Water temperature at 30 m is shown in panel d), and the mixed layer depth is indicated in panel e) (see Section 2.6 for details).

31

Supplementary Information:

- Figures S1-S169
- Comparison of conditions underlying measurements of primary productivity
- Treatment and calibration of ac-9 data (including Figures S120-S164 and Table S1)
-
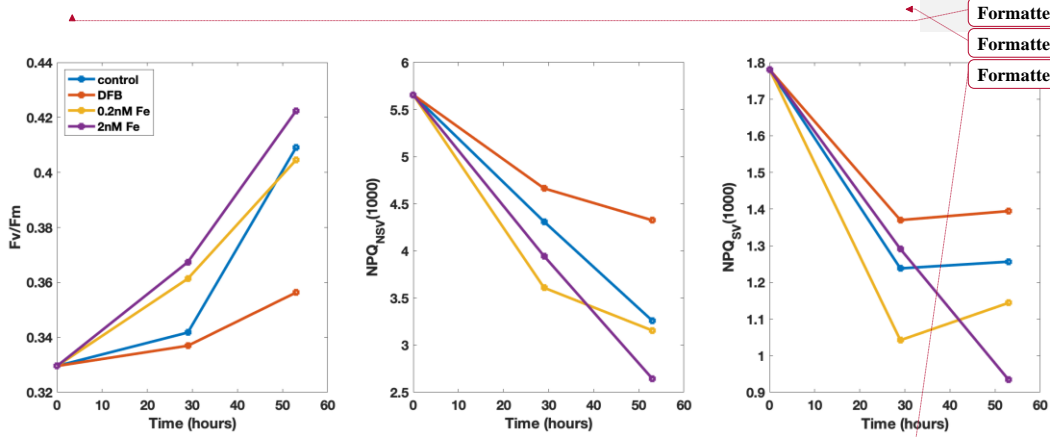
Figure S1: Time course of Fv/Fm as well as the two NPQ parameters for incubation 1, showing the results at the end point (after 52 h) as well as at 29 h. Colors represent different treatments as indicated in the figure legend. It is evident that the changes observed at 52 h were already underway at 29 h, but were generally more pronounced after 52 h.
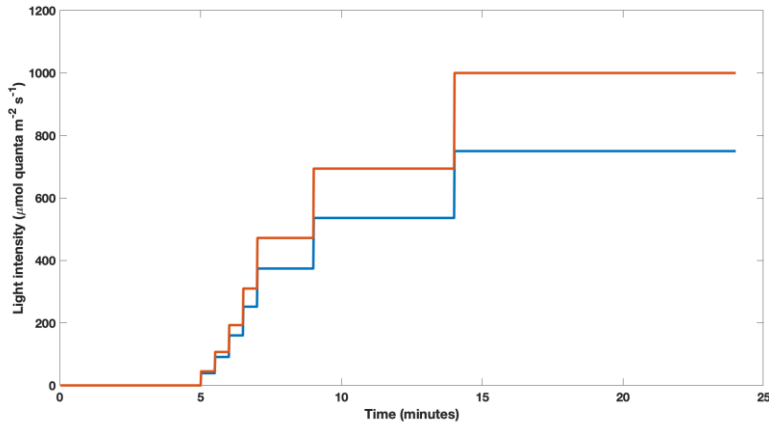
Figure S2: Schematic of time steps and light levels in fluorescence light curves employed in this study. The blue line relates to underway samples (with maximum light level of 750 μmol quanta m^{-2} s^{-1}) and the red line refers to samples from the deckboard incubation with maximum light levels of 1000 μmol quanta m^{-2} s^{-1}. The different maximum light intensities were chosen such that maximum NPQ was achieved for each set of samples, while still providing an induction curve in the FRRf that ~~cut~~could be readily fit to the expected functionality, (at higher light intensities the curve becomes too flat to achieve a good fit). Phytoplankton in the incubations ~~were able to handle~~displayed variable fluorescence at higher light intensities than phytoplankton in the underway samples, most likely due to high-light acclimation in the incubated samples~~or~~.

2
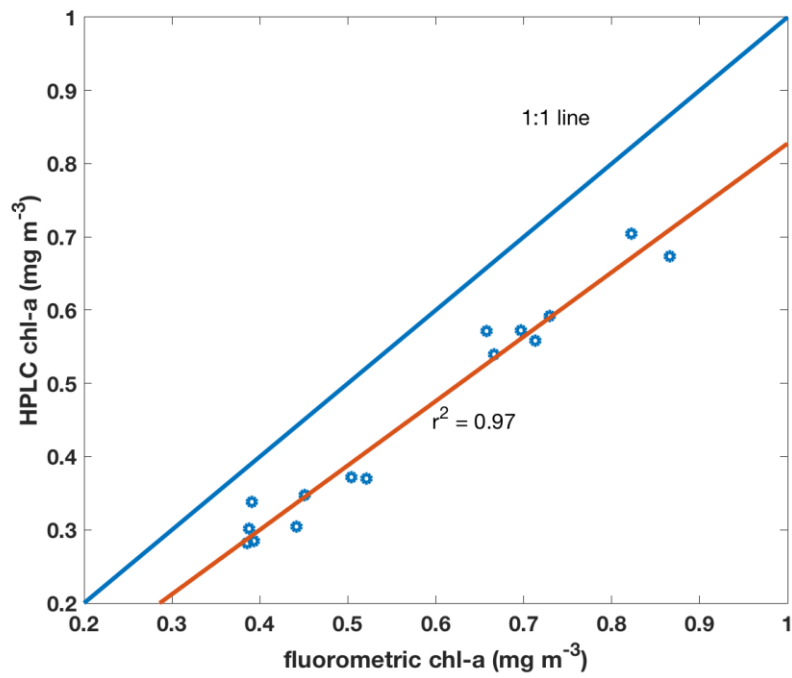
Figure S3S1: Comparison of Chl-a estimates from fluorometric analyses and HPLC. Linear regression yields the following expression: $Chl_{HPLC} = Chl_F * 0.879 - 0.052$ ($r^2 = 0.97$, n = 15, standard error of the estimate = 0.029 mg m^{-3}).
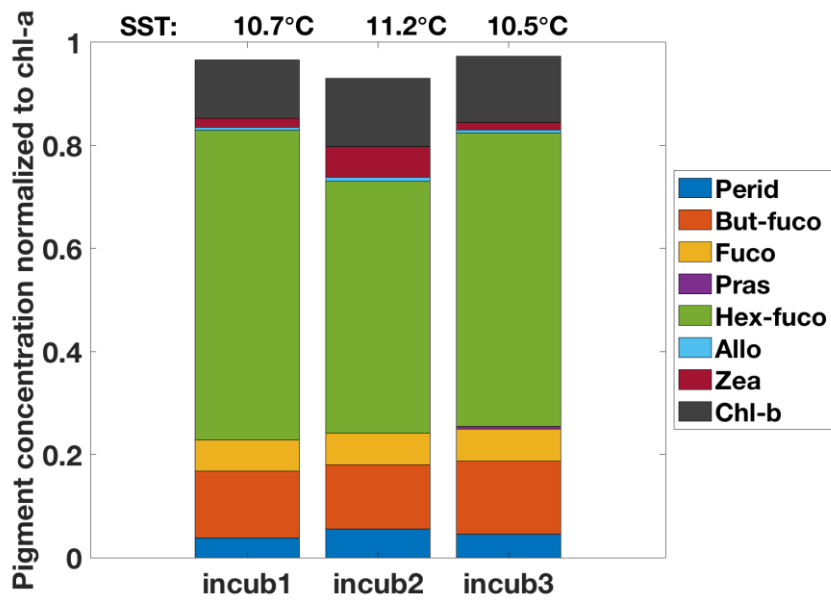
Figure S42: Initial pigment concentrations relative to Chl-a from HPLC analyses for the three incubation experiments. The sea surface temperature at time of sampling is indicated at the top. The HPLC analyses indicate that the sampled waters were dominated by haptophytes. S, and some diatoms and chrysophytes may also have been present.
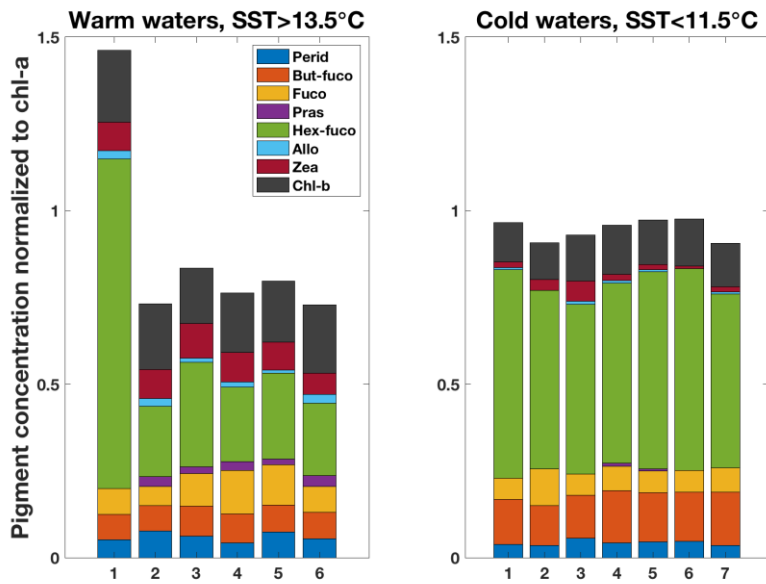
Figure S53: Pigment concentrations relative to Chl-a from HPLC analyses ~~for~~ of underway samples, grouped by SST. The HPLC analyses indicate that the cold waters were dominated by haptophytes, and some diatoms and chrysophytes may also have been present. Haptophytes, as indicated by the presence of Hex-fuco, were also present in the warm water mass, but they were less dominant here than in the cold waters. The warm waters also hosted some green algae (prasinophyt~~h~~es) and likely some diatoms, and some cyanobacteria may have been present, most likely *Synechococcus*. The data suggest that both the warm and cold waters had mostly similar phytoplankton sizes, except for the possibility of *Synechococcus* in the warm waters.
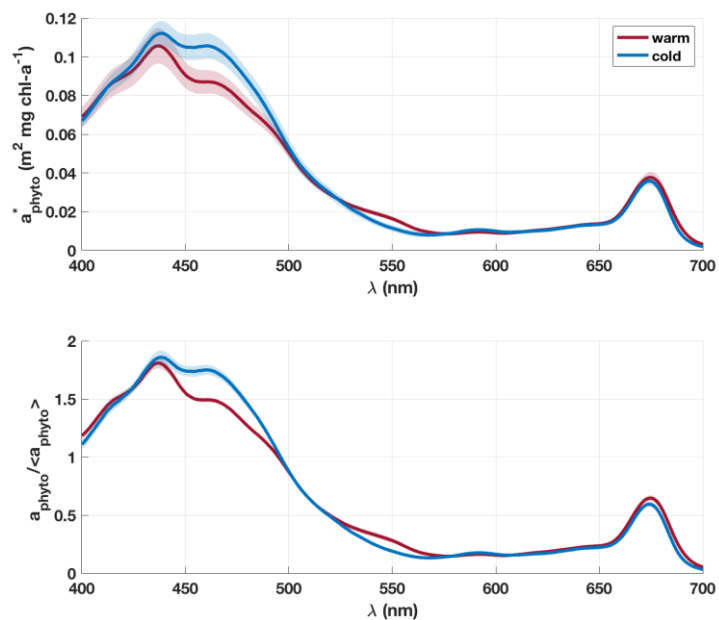
Figure S64: Mean phytoplankton absorption spectra for the respective water masses (~~indicated by~~red = warm; blue = ~~and~~ cold ~~colours~~) from underway samples (n=17), with one standard deviation indicated by shaded areas. Top panel shows phytoplankton absorption spectra normalized to the respective Chl-a concentrations, while the bottom panel shows phytoplankton absorption spectra normalized to the mean absorption $\langle a_{phyto} \rangle$.
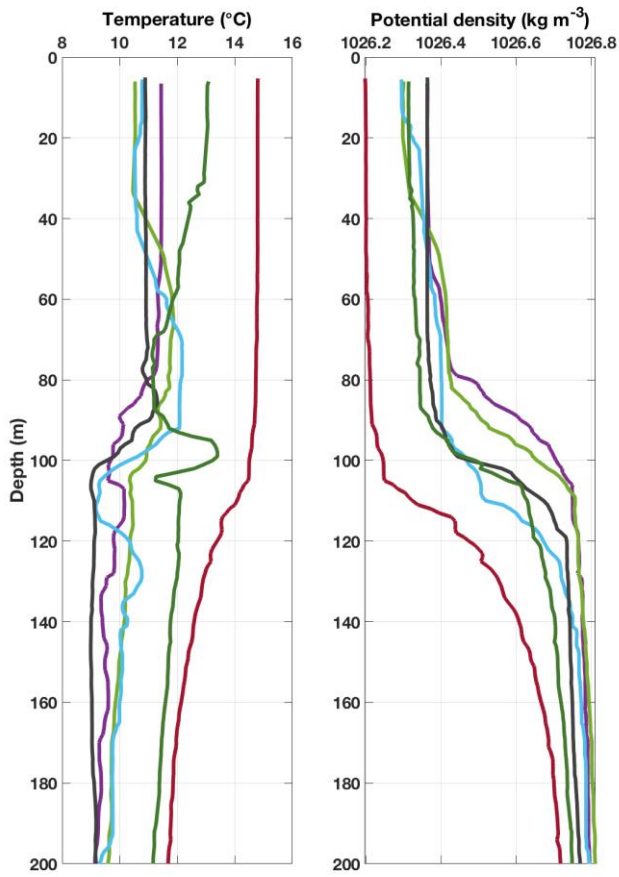
Figure S75: Temperature and density profiles from CTD casts on the SOTS voyage in 2018. The red line is the only profile from the warm water mass (SST>13.5°C), and the dark green profile was likely measured in a transitional zone. All other profiles are from the cold water mass and show varying mixed layer depths.
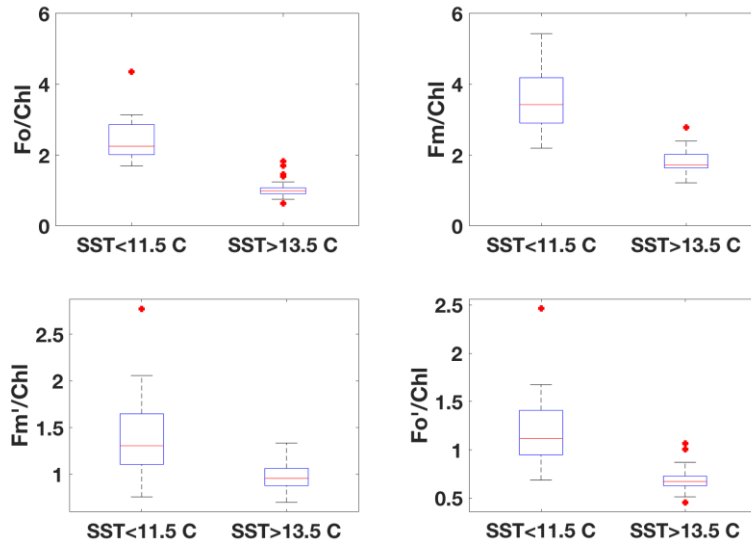
Figure S86: Individual fluorescence parameters measured with the FRRf on underway samples, normalized to Chl-a and grouped by SST. The minimum and maximum fluorescence in the dark-adapted state (F_o and F_m) are shown in the top panels, while the respective measurements in the light-acclimated state (in this case at 750 μmol quanta m^{-2} s^{-1}) are shown at the bottom. All parameters are significantly different ($p \ll 0.01$) between the two water masses.
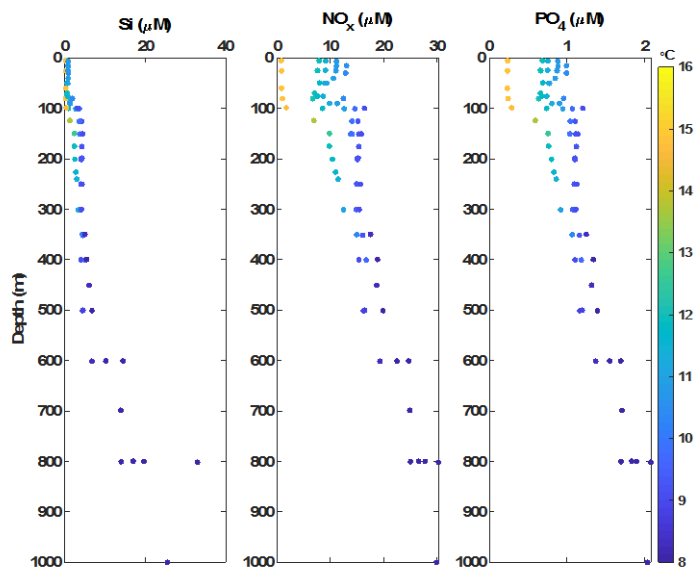
Figure S97: Profiles of macronutrient concentrations measured on the SOTS voyage in 2018, colour-coded by the respective temperature. Only one profile was measured in the warm water mass (yellow colours at the surface), exhibiting significantly lower NO_x and PO_4 concentrations than the colder water mass.
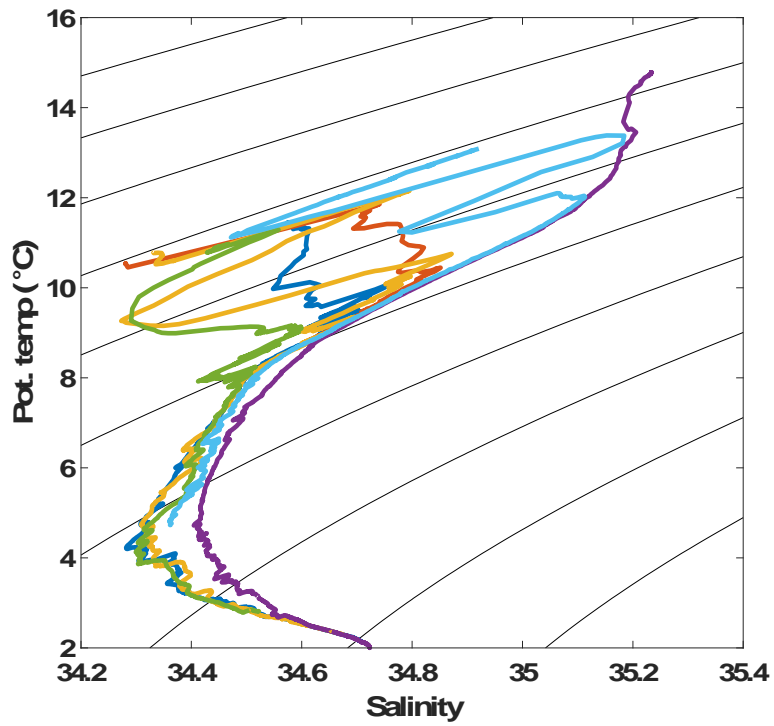
Figure S108: Temperature-salinity diagram for CTD data from the SOTS 2018 voyage. The purple line indicates data from the water mass with a warmer SST signature. This water mass also exhibited a saltier salinity minimum at depth, consistent with this water mass originating further north than the subantarctic Subantarctic cold water mass (Herraiz-Borreguero & Rintoul, 2011).
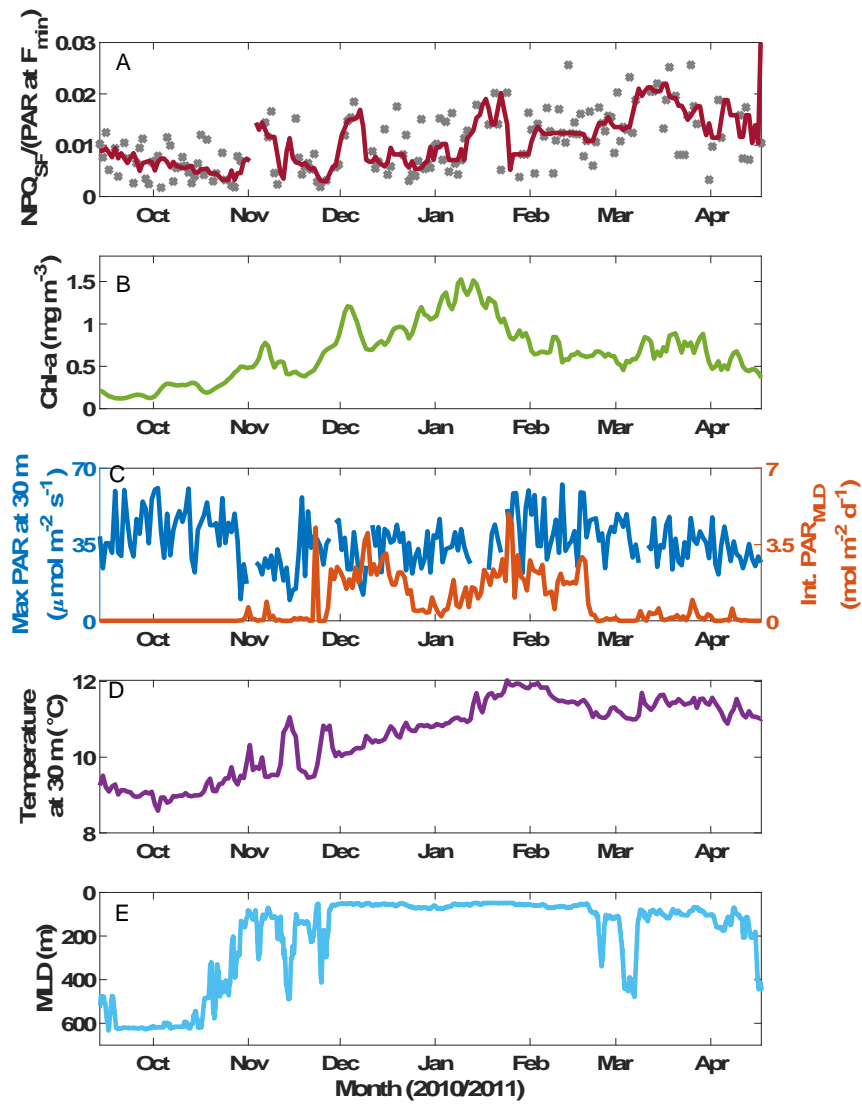
Figure S119: SOTS mooring data for October 2010 to April 2011; same as Figure 9 in the main manuscript except for panel A. Here, panel A shows NPQ_{SF} normalized to PAR at F_{min}, with grey markers indicating daily estimates and the red line a 7-day running median. Panel B shows a 3-point running mean over daily Chl-a concentrations estimated based on calibrated fluorescence; panel C shows maximum PAR recorded at 30 m for any given day (left axis) and the integrated daily PAR for the mixed layer (right axis). Water temperature at 30 m is shown in panel D, and the mixed layer depth is indicated in panel E.

Comparison of conditions underlying measurements of primary productivity:

Our discussion in Section 3.2.4 compares findings regarding primary productivity between our study and that of Westwood et al. (2011). A number of factors can contribute to the observed differences in primary productivity, hence we compare the conditions found in the two studies in order to pinpoint the most likely candidate. Sea surface temperatures were similar between Westwood et al. (2011) and our study (12°C vs 11°C, respectively), mixed layer depths were also similar (mean=38 +/- 11 m and mean=35 +/- 1 m, respectively), but the column-integrated Chl-a was different: mean=46 +/- 11 mg m^{-2} vs mean=13 mg m^{-2}. However, the fact that biomass was lower in our study could also be the result of lower iron concentrations (and lower rates of primary productivity). Moreover, normalizing the mean column-integrated primary productivity for each study by the mean column-integrated Chl-a concentration yields 85 mg C (mg Chl)$^{-1}$ d^{-1} for Westwood et al. (2011) and 31 mg C (mg Chl)$^{-1}$ d^{-1} for our study, indicating that the Chl-normalized primary productivity was lower during our study (in Austral fall) than in the Westwood et al. study in Austral summer. The conclusion that primary productivity was lower in our study thus holds, with ~~iron~~Fe limitation a probable cause, as discussed in Section 3.2.4.

Treatment and calibration of ac-9 data:

The largest problem encountered on the cruise was the presence of bubbles in the flow tubes, as has been reported previously (Slade et al., 2010). This problem was intermittent, i.e. there were whole multi-hour stretches without bubbles, but overall the problem persisted through the duration of the cruise. In order to make the most of the data, the raw data (file by file and wavelength by wavelength, both filtered and unfiltered) were processed as follows:

1) A moving standard deviation for 1 minute of data (359 data points) was calculated for each file, and at the end the median of that standard deviation was calculated (stdev).

2) A running median (1-minute, i.e. 359 data points) was then calculated, and any raw values that fell outside the envelope defined by the median +/-3*stdev were flagged as bubbles and removed from further processing.

3) A running median was calculated of the remaining data over a 999-point window (<3 minutes), and these smoothed data were binned into 1-minute medians.

4) The filtered data were interpolated based on the corresponding time stamps to match the unfiltered data and were then subtracted from the unfiltered data, yielding particulate absorption (a_P). This step, in principle, accounts for issues relating to absolute calibration of the absorption channels such as dependence on the clean water offset as well as temperature and salinity corrections (e.g., Slade et al. 2010). However, in practice there will still be temperature offsets (i.e., the filtered and unfiltered measurements cannot be expected to have been at the exact same temperatures), and there is also an over-estimation of absorption in reflective flow tubes that should be accounted for with a scattering correction (Slade et al. 2010). The limited wavelengths of the ac-9 make a comprehensive temperature and scattering correction – such as is recommended for hyperspectral instruments – impossible. We thus opted to not apply any further corrections, noting that the expected uncertainty due to this omission is ~$0.006\Delta T$ at λ=412 nm, and less at longer wavelengths (Slade et al. 2010).

5) Particulate absorption line height at 676 nm (LH(676), m^{-1}) was then calculated following Roesler and Barnard (2013), subtracting a baseline based on absorption measurements at 650 and 715 nm.

6) Before calibrating the ac-9 data against discrete Chl-a and phytoplankton absorption measurements from filter pad, the LH(676) time series was further smoothed with a 1-hour running median to reduce residual noise. This step considerably improved calibrations for both Chl-a and mean phytoplankton absorption $<a_{phyto}>$ (see Figures and Table below).
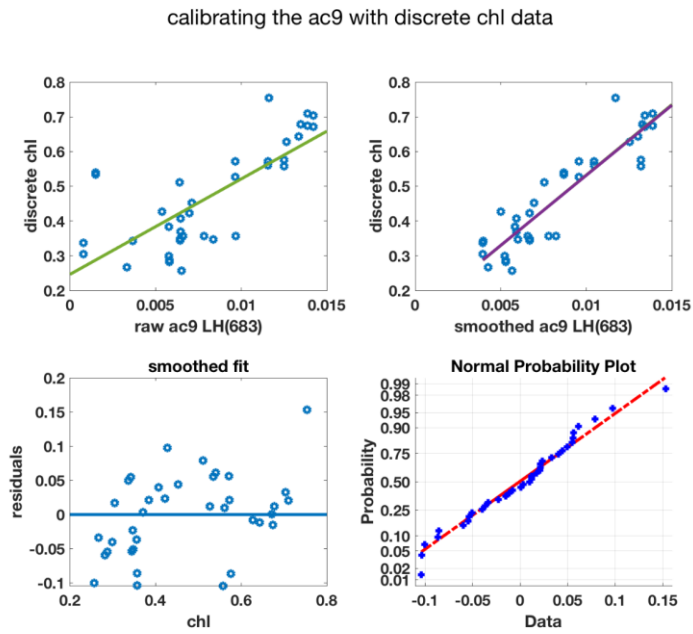
calibrating the ac9 with discrete chl data

Figure S12: Calibration of ac-9 line height (LH(676)) against discrete Chl-a (HPLC and fluorometric samples combined). Top panels: Calibrations for raw (left) and smoothed (right) ac-9 data (1-hr running median), with regression lines indicated in green and purple. Bottom: Residuals of the regression with smoothed ac-9 data as a function of Chl-a, and normal probability plot of the same residuals. See Table S1 for statistics and calibration coefficients.
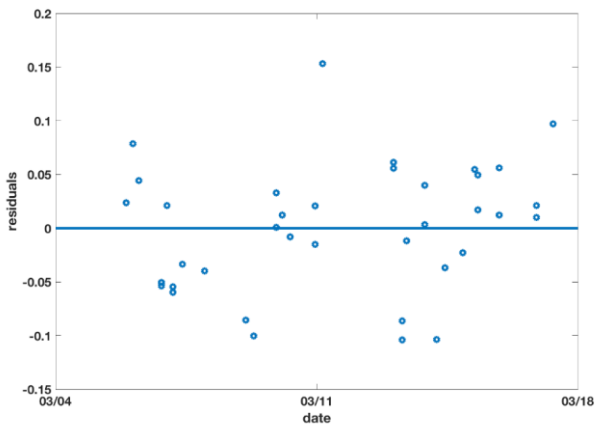

Figure S13: Residuals of the smoothed calibration of ac-9 line height (LH(676)) against discrete Chl-a (see above) as a function of time, showing no evidence of bio-fouling.
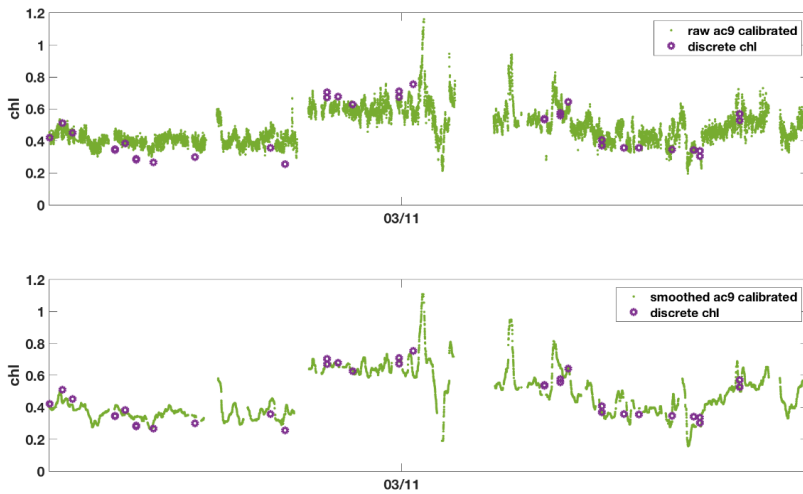
Figure S1~~4~~2: Calibrated ac-9 data (green) overlain with discrete Chl-a samples (purple). ac-9 data calibrated as indicated in Figure S10 and Table S1, i.e. using the raw and smoothed ac-9 data respectively. Top panel shows the raw ac-9 data and bottom-panel shows the smoothed ac-9 data (1-hr running median). It is evident that the smoothing improves the match-ups.
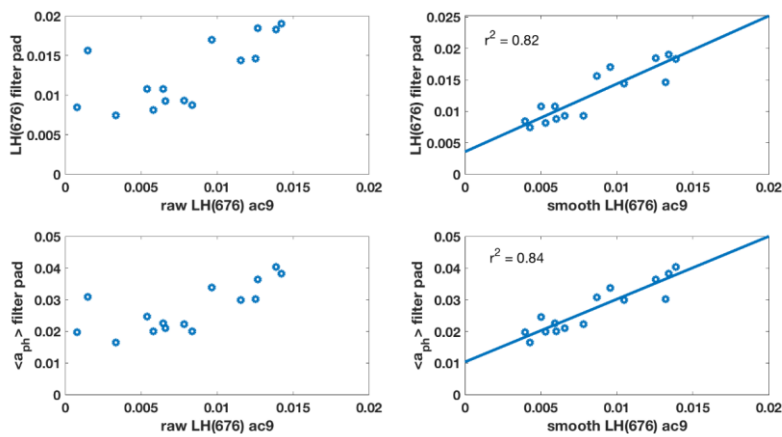

Figure S1~~5~~3: Relationship between raw (left) and smoothed (right) ac-9 LH(676) and phytoplankton absorption measurements from filter pad analyses. Top panels show relationships to LH(676) from filter pad absorption, bottom panels show relationships with mean phytoplankton absorption <a_{ph}> from filter pads. Linear regression lines only shown for smoothed ac-9 data.
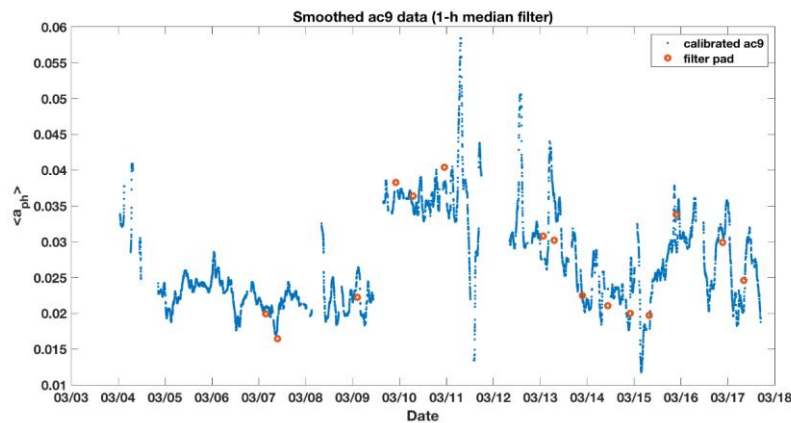
Figure S164: Calibrated ac-9 time series (smoothed with a 1-hr running median) of mean absorption $\langle a_{ph} \rangle$ in blue, with discrete filter pad measurements of $\langle a_{ph} \rangle$ overlain in red.

Table S1. Statistics of the respective ac-9 calibrations:

LH(676) ac-9 against:	r^2 raw	SEE raw	Slope raw	Intercept raw	r^2 smoothed	SEE smoothed	Slope smooth	Intercept smoothed
Chl-a	0.56	0.15	27.47	0.246	0.84	0.07	40.56	0.127
LH(676) filter pad	0.48	0.004	0.68	0.007	0.82	0.002	1.08	0.004
$\langle a_{ph} \rangle$ filter pad	0.54	0.009	1.30	0.017	0.84	0.005	1.99	0.010

SEE = standard error of the estimate

References

Herraiz-Borreguero, L., and Rintoul, S. R.: Regional circulation and its impact on upper ocean variability south of Tasmania. Deep-Sea Res. Pt. II, 58(21–22), 2071–2081, https://doi.org/10.1016/j.dsr2.2011.05.022, 2011.

Roesler, C. S., and Barnard, A. H.: Optical proxy for phytoplankton biomass in the absence of photophysiology: Rethinking the absorption line height. Methods in Oceanography, 7, 79–94, https://doi.org/10.1016/j.mio.2013.12.003, 2013.

Slade, W., Boss, E., Dall'Olmo, G., Langner, M., Loftin, J., Behrenfeld, M., … Westberry, T.: Underway and moored methods for improving accuracy in measurement of spectral particulate absorption and attenuation. J. Atmos. Oceanic Tech., 27, 1733–1746, https://doi.org/10.1175/2010JTECHO755.1, 2010.

Westwood, K. J., Griffiths, F. B., Webb, J. P., and Wright, S. W.: Primary production in the Sub-Antarctic and Polar Frontal Zones south of Tasmania, Australia; SAZ-Sense survey, 2007. Deep-Sea Res. Pt. II, 58, 2162–2178, 2011.